



HAL
open science

Adsorption of arabinogalactan-proteins from Acacia gums (senegal and seyal) and its molecular fractions onto latex particles

Didier Renard, A. Davantès, A. d'Orlando, K. Cahier, M. Molinari, Michael Nigen, P. Chalier, C. Sanchez

► To cite this version:

Didier Renard, A. Davantès, A. d'Orlando, K. Cahier, M. Molinari, et al.. Adsorption of arabinogalactan-proteins from Acacia gums (senegal and seyal) and its molecular fractions onto latex particles. *Food Hydrocolloids*, 2022, 125, pp.107360. 10.1016/j.foodhyd.2021.107360 . hal-03540576

HAL Id: hal-03540576

<https://hal.inrae.fr/hal-03540576v1>

Submitted on 22 Jul 2024

HAL is a multi-disciplinary open access archive for the deposit and dissemination of scientific research documents, whether they are published or not. The documents may come from teaching and research institutions in France or abroad, or from public or private research centers.

L'archive ouverte pluridisciplinaire **HAL**, est destinée au dépôt et à la diffusion de documents scientifiques de niveau recherche, publiés ou non, émanant des établissements d'enseignement et de recherche français ou étrangers, des laboratoires publics ou privés.



Distributed under a Creative Commons Attribution - NonCommercial 4.0 International License

Adsorption of arabinogalactan-proteins from *Acacia* gums (*senegal* and *seyal*) and its molecular fractions onto latex particles

D. Renard^{*a}, A. Davantès^a, A. D'orlando^a, K. Cahier^a, M. Molinari^b, M. Nigen^c, P. Chalier^c, C. Sanchez^c

^a INRAE UR 1268 BIA 44 300 Nantes France; * denis.renard@inrae.fr

^b CBMN, CNRS UMR 5248, IPB, Université de Bordeaux, Pessac, France

^c UMR 1208 IATE 34 060 Montpellier Cedex 1 France

Abstract

Adsorption of Acacia gums (GA) (*A. senegal* and *A. seyal*) and *A. senegal* molecular fractions, made of arabinogalactan-proteins (AGPs) with different molecular weights, onto latex particles, with different sizes and surface charges, was studied using molecular (fluorescence and nanoIR spectroscopies, microscopies including Atomic Force Microscopy) and mesoscopic (Dynamic Light Scattering, zeta potential, Asymmetrical flow field-flow fractionation) methods. Adsorption of GA onto latex particles revealed a complex mechanism of adsorption where the highest adsorption was observed when *A. senegal* and latex particles were negatively charged. The invert was observed for *A. seyal* where the maximum of adsorption was observed when gum and latex were oppositely charged. The duality of positive and negative charges on GA macromolecules together with conformational changes certainly explain the complex mechanism of adsorption. A mechanism where either the protein moiety either the sugars blocks adsorb is to be preferred. This mechanism seems to produce differences of behaviour due to viscoelastic properties of adsorbed layers, and differences of hydration due to differences of polarity of AGPs. The consequence of electrostatics in the adsorption process is a water release from the adsorbed layers and important gain in entropy. A fair agreement was found between protein content and adsorbed layer thickness of GA, with the formation of partial coverage, monolayer and multilayer films depending on GA concentration. Structural changes induced by GA adsorption onto latex particles was probed using fluorescence and nanoIR spectroscopies without giving clear evidence of conformational changes induced after GA adsorption. The results of this study highlighted that GA surface adsorption process depend not only on the protein moiety and electrostatic interactions but also on other parameters related to AGP hydration status. The protein structural accessibility, the molecular weight distribution, the AGPs intrinsic viscoelastic properties allowing structural rearrangements on the surface and spreading in order to form a viscoelastic film onto latex particles should also play a pivotal role in the adsorption process.

Key words. *Acacia* gum, arabinogalactan-protein, adsorption, latex, nanoinfrared atomic force microscopy.

1. Introduction

Acacia gum (GA), also called gum Arabic, is the oldest and, apparently, best known of all natural gums (Sanchez, et al., 2018; Verbeken, Dierckx, & Dewettinck, 2003). It is an edible dried gummy exudate obtained from the trunk and branches of *Acacia senegal* and *Acacia seyal* trees. The gum production, i.e. gummosis, is a protection mechanism of tree against insect and mold invasion, which participate to the healing of wounds.

GA is a highly heterogeneous material that can be separated into three main fractions by hydrophobic interaction chromatography (HIC): an arabinogalactan-peptide (AGp), an arabinogalactan-protein (AGP) and a glycoprotein (GP) molecular fractions (Renard, Lavenant-Gourgeon, Ralet, & Sanchez, 2006). They have a similar carbohydrate composition, especially AGp and AGP, but differ by their protein content, amino acid composition, and molecular weight distribution. Protein content was found to be made of polypeptides, rich in hydroxyproline (Hyp), serine (Ser) and threonine (Thr) residues, with molecular weights varying from 5.10^3 g.mol⁻¹ (Mahendran, Williams, Phillips, Al-Assaf, & Baldwin, 2008; Renard, et al., 2006) up to $4.8.10^5$ g.mol⁻¹ (Renard, et al., 2006). Many authors identified several bands by gel electrophoresis, with or without deglycosylation treatment, meaning that molecular fractions of GA should differ in polypeptidic length and that proteins alone (without glycosylation) should also exist (Hippolyte, 1998; Mahendran, et al., 2008; Motlagh, Ravines, Karamallah, & Ma, 2006; Osman, Menzies, Williams, Phillips, & Baldwin, 1993; Renard, et al., 2006).

Functional properties of GA are numerous and widely used in different food and non-food applications (Verbeken, et al., 2003). Amongst these properties, surface properties of AG are unique in the polysaccharide world. By surface properties, it means both the ability to decrease interfacial tension between gas-liquid, liquid-liquid or solid-liquid interfaces, and to stabilize these interfaces through steric and electrostatic interactions and hydration forces (Adamson & Gast, 1997). GA is therefore widely used to stabilize foams (Redgwell, Schmitt, Beaulieu, & Curti, 2005), emulsions (Buffo & Reineccius, 2000) and various solid nanoparticles (Sanchez, et al., 2018). Obviously, the ability of GA to stabilize solid interfaces was at the basis of ink and paint manufacturing (Balantrapu & Goia, 2009; Song, Choi, & Chin, 2007; D. W. Wang & Zhao, 2009). GA was also used to stabilize latex nanoparticles as a model system of interface with a surface coverage of about 0.5 – 5 mg.m⁻² depending on solvent conditions and initial GA concentration (Gashua, Williams, & Baldwin, 2016; Sanchez, et al., 2018; Snowden, Phillips, & Williams, 1987). The surface coverage was found to be similar at liquid-liquid interfaces in O/W emulsions (Randall, Phillips, & Williams, 1988). The protein-rich high-molecular weight fraction of GA, GP, was found to be the most effective to be adsorbed at the interface and it was demonstrated, using electron spin resonance, that GA adsorbed at the solid-liquid interface with approximately half of its segments close to the surface in trains and the other half in loops and tails extending away from the surface into solution (Sanchez, et al., 2018; Snowden, et al., 1987). An alternative model of end-on or multilayer adsorption was recently proposed to explain the high layer thickness after adsorption of GA on latex nanoparticles (Gashua, et al., 2016). The adsorption onto latex was completed after 4 days and 100% of the proteinaceous material was adsorbed (Snowden, et al., 1987; Snowden, Phillips, & Williams, 1988) whereas only 25% of the proteinaceous material was adsorbed to orange oil droplets (Randall, et al., 1988). In addition, it was found that the adsorption of the high molecular weight protein fractions of *A. seyal* onto an oil droplet was found not to be a highly efficient emulsifying component. Structurally, while *A. seyal* may have the same core structural linkages as *A. senegal*, the degree of branching is greater, with the protein distributed differently (Flindt, Al-Assaf, Phillips, & Williams, 2005).

Recent study on GA adsorption on solid surfaces using quartz crystal microbalance with dissipation monitoring (QCM-D) and surface plasmon resonance (SPR) revealed that 3.3 fold more AGPs from *A. seyal* (500 ppm) are needed to cover the gold surface compared to *A. senegal* (150 ppm) (Davantes, Nigen, Sanchez, D'Orlando, & Renard, 2019). This is to be related to the ~2 fold more protein content in *A. senegal*. The pH and salt concentration of the environment greatly affected the adsorption behavior of both gums, with the surface density ranging from 0.92 to 3.83 mg m⁻² using SPR (i.e., “dry” mass) and from 1.16 to 19.07 mg m⁻² using QCM-D (wet mass).

Literature gave many assumptions regarding the molecular basis of adsorption in particular at liquid-liquid interfaces (Aphibanthammakit, Barbar, Nigen, Sanchez, & Chalier, 2020; Dickinson, Galazka, & Anderson, 1991; Dickinson, Murray, Stainsby, & Anderson, 1988; Jayme, Dunstan, & Gee, 1999; Nishino, Katayama, Sakata, Al-Assaf, & Phillips, 2012; Yadav, Igartuburu, Yan, & Nothnagel, 2007). A preferential adsorption onto oil-water interfaces of protein-rich fractions was clearly demonstrated. However, all molecular fractions of GA seems to be present at interfaces, with different adsorption kinetics (Alftren, Penarrieta, Bergenstahl, & Nilsson, 2012; Atgie, Chenneviere, Masbernat, & Roger, 2019; Atgie, Masbernat, & Roger, 2019; Flindt, et al., 2005). However, new studies on structural changes occurring after GA adsorption onto liquid and solid interfaces could therefore help to a better understanding on which part of GA is preferentially adsorbed and/or whether conformational changes occur after adsorption.

The aim of the present study was therefore to focus on the composition-structure-function relationships of arabinogalactan-proteins from *Acacia* gums (*A. senegal* and *A. seyal*) at solid-liquid interfaces. Few information is presently available on the behaviour and conformation of these arabinogalactan-protein macromolecules at solid-liquid interfaces (Aphibanthammakit, Nigen, Gaucel, Sanchez, & Chalier, 2018). By tuning the chemical composition of arabinogalactan-proteins fractions, we aim at deeply understanding the mechanisms of adsorption and the forces involved in the adsorption process. The present study highlights the evolution and characterization of the adsorbed polysaccharide layer and potential conformational changes induced by the adsorption onto solid particles (negatively and positively charged polystyrene latex beads). The adsorption polysaccharide layer was characterized using dynamic light scattering (DLS) and mobility measurements together with several microscopic techniques (Scanning Electron Microscopy (SEM), Transmission Electron Microscopy (TEM), Scanning Transmission Electron Microscopy (STEM), Atomic Force Microscopy (AFM)). A recent microscopic technique, AFM coupled to infrared spectroscopy, was also used in order to evidence the adsorption of GA on latex nanoparticles after dehydration of the material. Further characterization of the adsorbed polysaccharide layer used Asymmetrical Flow Field-Flow Fractionation (A4F) with Multi-Angle Laser Light Scattering (MALLS) detection technique to estimate the mass of polysaccharide, and consequently, the number of macromolecules adsorbed onto latex particles. Conformational changes after adsorption were finally probed using front-face fluorescence spectroscopy in steady state and time-resolved modes.

2. Materials and methods

2.1. Materials

Instant and soluble *Acacia senegal* (SN) Lot N°OF152413 and *Acacia seyal* (SY) Lot N° OF110724 gum powders were supplied by ALLAND & ROBERT Company – Natural and organic gums (Port Mort, France). Raw nodules of *A. senegal* and *A. seyal* gums were collected in Sudan in 2011. Both *Acacia* gums followed the same purification process: elimination of insoluble

materials by physical methods, pasteurisation, and spray drying. Molecular fractions from *Acacia senegal* were purified by hydrophobic interaction chromatography (HIC), as previously described (Renard, et al., 2006). Purified fractions, named HIC-FI, HIC-FII and HIC-FIII, were dialysed and freeze-dried before further use. A summary of the protein content, molar mass and sphere-equivalent hydrodynamic diameter of samples used in this study are displayed in Table 1 (Lopez-Torrez, Nigen, Williams, Doco, & Sanchez, 2015; Renard, et al., 2006). **These fractions, purified few years ago, were checked every six months by HPSEC-MALLS in order to confirm the absence of chemical or bacterial degradation.**

Polystyrene latex particles of 0.1 μm mean particle size were purchased from Sigma-Aldrich (Ref. LB1-2ML); they were in the form of a 10% aqueous dispersion with $1.8 \cdot 10^{14}$ particles/mL. Amino polystyrene latex particles of 0.5 μm mean particle size were purchased from Polysciences (Ref. 07763); they were in the form of a 2.5% aqueous dispersion with $3.6 \cdot 10^{11}$ particles/mL. Carboxyl (Ref. C37485) and amidine (Ref. A37313) latex particles of 0.1 μm mean particle size were purchased from Invitrogen; they were in the form of a 4% aqueous dispersion with $7.3 \cdot 10^{13}$ particles/mL.

2.2. Gum dispersions preparation

Acacia senegal, *Acacia seyal*, HIC-FI, HIC-FII and HIC-FIII dispersions were prepared in deionized water at 1% w/w. The completely hydrated dispersions were centrifuged at 5 000 rpm for 20 min at 25°C to remove the insoluble part. The supernatant was collected and was used for the preparation of latex-gum dispersions.

2.3. Latex-gum dispersions preparation

9.5 mL of total gums or molecular fraction dispersions at concentrations of 0.1 or 0.5 g/L were added to 0.5 mL of a 5 g/L polystyrene latex dispersions corresponding to a final gum concentration of 0.095 g/L (95 ppm) or 0.475 g/L (475 ppm) and a final latex concentration of 0.25 g/L (250 ppm). For HIC-FIII, final concentrations of 0.03 g/L (30 ppm) and 0.1 g/L (100 ppm) were used due to the loss of material after centrifugation. The mixtures were then put on a rotating wheel for complete homogenization and equilibrium during all the duration of experiments (14 days). Total surface area available from 0.5 μm and 0.1 μm polystyrene latex dispersions in 10 mL were of 7.2 and 11.4 cm^2 , respectively.

2.4. Methods

2.4.1. Dynamic Light Scattering (DLS)

The sphere-equivalent hydrodynamic diameter (D_h , with $D_h = 2R_h$) of latex particles, free and in presence of total gums or molecular fractions, was determined by DLS (Zetasizer, Nano series, Malvern Instruments). Measurements were carried out at $T = 25^\circ\text{C}$ after 2 min of equilibration time in plastic cuvettes ($V = 2 \text{ mL}$) at a scattering angle $\theta = 173^\circ$, a detector position fixed at 4.65 mm and an attenuation factor of 6 (or 7). Three runs of 60 s each were performed by sample. The light intensity fluctuations measured through the correlation function $g(\tau)$ were analysed using the **Cumulant** method to get the average hydrodynamic radii. The adsorbed layer thickness δ (nm) was calculated according to equation:

$$\delta = D_h^{adsorbed} - D_h^{free} \quad (2)$$

with $D_h^{adsorbed}$ the hydrodynamic diameter of the adsorbed polysaccharide latex particle and D_h^{free} the hydrodynamic diameter of the latex particle free of adsorbed polysaccharide. **Using this equation, it was supposed that aggregation and/or flocculation was neglected.**

2.4.2. Zeta potential

The zeta potential (ζ) measurements on latex dispersions were carried out at 25 °C using the Zetasizer Nano series (Malvern Instruments). Three measurements per sample were performed and the average electrophoretic mobility μ ($\mu\text{m}\cdot\text{cm}/\text{V}\cdot\text{s}$) of latex particles in water was converted to ζ potential (mV) using the von Smoluchowski equation:

$$\mu = \frac{\varepsilon\zeta}{\eta} \quad (3)$$

with ε and η the static permittivity and the viscosity of the solvent, respectively. The von Smoluchowski equation applies when $\kappa a \gg 1$, with a the radius of curvature (*i.e.* particle radius) and κ the Debye length. For latex particles of 0.1 μm and 0.5 μm in water, $\kappa a = 1.7$ and $\kappa a = 16.7$, respectively. **Analyses of electrophoretic mobility distribution was performed using the General purpose mode.**

2.4.3. Asymmetrical flow field-flow fractionation (A4F)

The A4F equipment, including the asymmetrical channel, Control-Box V3, Flow box P2.1, and the valve box, was obtained from Consensus (Ober-Hilbersheim, Germany). The channel geometry was trapezoidal with a tip-to-tip length of 286 mm and breadths at the inlet and outlet of 21.2 and 4.7 mm, respectively. A 350 μm polyester spacer and a regenerated cellulose membrane with a cutoff point of 10 000 Da from Celgard LLB (Charlotte, NC) were used. The A4F channel flow, cross flow, sample injection and focus flow were controlled with a Wyatt Eclipse A4F flow chassis, a pump and an autosampler from ThermoFisher Scientific (Waltham, MA, USA).

During all A4F experiments, the sample was introduced into the channel using a 100 μL loop injector (Valco Instruments Co., Inc., Houston, TX). Prior to use, the carrier (Millipore water containing 0.2 g/L sodium azide) was carefully degassed and filtered through Durapore GV (0.2 μm) membranes (Millipore). The carrier was eluted initially at a flow rate of 1 mL/min for channel flow in (F_{in}). The crossflow (F_c) was then set at 1 mL/min, and the channel flow rate (F_{out}) was set at 0.2 mL/min for the sample introduction and relaxation/focusing period. The filtrated (0.45 μm) 0.1 μm latex sample was injected at 0.14 mL/min for 160 s. After the injection pump was stopped, the sample was allowed to relax and focus for 60 s. For elution, F_{out} was set at 1 mL/min, and F_c was reduced from 0.4 to 0 mL/min for 400 s, after which it was maintained at 0 mL/min for 875 s. Sample recoveries were calculated from the ratio of the mass eluted from the channel (integration of the DRI signal) and the injected mass. The A4F instrument was coupled with two on-line detectors: a MALLS instrument (DAWN Heleos II) fitted with a K5 flow cell and a He-Ne laser ($\lambda = 663 \text{ nm}$), and a refractometric detector operating at the same wavelength (Optilab T-rEX) from Wyatt Technology (Santa Barbara, CA, USA). The molecular weight (M_w), the molecular dispersity (M_w/M_n), and the radius of gyration (R_g) were determined with Wyatt ASTRA® software (v. 6.1.4.25) excepted that ten angles were used (from 37.5 to 120.1°) for Berry extrapolation. The refractive index increment dn/dc of latex particles was of 0.226 mL/g, value determined at $T = 25 \text{ °C}$ on an independent refractometer operating at $\lambda = 589 \text{ nm}$.

2.4.4. Infrared spectroscopy

Infrared spectra were performed on a Thermo Nicolet IS50 spectrometer (Thermo Scientific) in the wavenumber range ranging from 4000 to 400 cm^{-1} with a resolution of 16 cm^{-1} using a DGTS detector. Samples were prepared in KBr pellets by mixing 2 mg of sample with 120 mg of KBr. Results were obtained using the OMNIC software (v. 9.2.41).

2.4.5. Microscopy

2.4.5.1. NanoInfrared Spectroscopy

AFM experiments coupled to infrared spectroscopy and imaging (NanoIR) were performed using a NanoIR2 system (Bruker, Santa Barbara, United States). Thanks to the use of the AFM probe to detect the IR absorption by a sample, the nanoIR technology allows to improve the lateral resolution to around ten nanometers compared to classical IR, and to locally acquire a IR spectrum or to perform imaging at a given wavenumber. The nanoIR principles are now well mastered and the technology allows having a very important sensitivity by using proper substrates, probes, and excitation laser (Dazzi, et al., 2012; Kurouski, Dazzi, Zenobi, & Centrone, 2020).

To perform the experiments, a drop of the different samples was deposited onto an IR transparent substrate of ZnSe and dried in ambient conditions. The different analyses were performed using PR-EX-nIR2 cantilevers (Bruker, Santa Barbara, United States) with a nominal spring constant of 0.07–0.4 N.m^{-1} and nominal radius of 20 nm, The excitation was performed using a Quantum Cascade Laser (QCL) (Ekspla, Lithuania) with 4 chips covering a wavenumber range from 1000 cm^{-1} to 2000 cm^{-1} .

In the spectroscopic mode, a local IR spectrum was recorded at a given point of the samples selected after acquiring a classical AFM image and then by tuning the laser over its wavelength range. For the experiments, spectra with a resolution of 4 cm^{-1} were acquired and around 20 spectra per point were summed to have an average signal with a good signal/noise ratio and at least 10 different points per samples were studied to ensure the reproducibility of the measurements. Compared to classical IR measurements, and due to the difference in the excitation and detection chains, some band intensities could be more or less important in the nanoIR spectra but the relative intensities between different spectra could be compared. For the purpose of the study and to emphasize the presence of the Acacia gum signal, the amplitude of the band at 1493 cm^{-1} , characteristic of the latex, has been used to normalize the different spectra and fixed to an arbitrary intensity of 1 for all the measurements.

After acquiring spectra on a sample, an IR intensity map at a given wavenumber was acquired by selecting characteristic wavenumbers for the latex, *A. senegal* and *A. seyal*. The characteristic bands were selected at 1493, 1654, and 1658 cm^{-1} , respectively, thanks to a study of the reference samples (bare latex particles, *A. senegal* and *A. seyal* samples). To avoid artefacts that could come from the topography of the sample surface, the resonant contact mode was used for the IR mapping.

Measurements of the aqueous latex dispersions, *A. senegal* solutions, and the fonctionnalised latex dispersions were performed at ambient temperature with a controlled humidity of 35%.

2.4.5.2. Scanning transmission electron microscopy (STEM)

Wet-STEM is a transmission imaging mode allowing the examination of nano-objects suspended in a liquid phase. Wet-STEM observations were made on hydrated bare

latex (0.025%) and *A. senegal* (0.95%) adsorbed onto carboxy latex particles after 100 fold dilution, using an environmental scanning electron microscope (ESEM, Quattro S, Thermo Scientific, US). Images were obtained under environmental conditions without any sputter-coating of the specimens (3°C and pressure varying between 300Pa and 700Pa, resulting in a humidity from 40% to 90% RH). An accelerating voltage of 20kV was used with a bright field STEM detector. This method discards artefacts that comes from observations made after a dehydration step of the samples before microscopic observations.

3. Results

3.1. Adsorbed layer thickness: *adsorption vs flocculation*

To probe adsorption of gums and molecular fractions at solid-liquid interface, first results dealt with the adsorbed layer thickness determination of gums adsorbed onto polystyrene latex particles (Sigma-Aldrich) of 0.1 μm in presence of 0.5M NaCl. Results clearly revealed the flocculation of latex particles free of adsorbed gums in presence of salt (the average hydrodynamic diameter D_h increased from 0.1 μm to 3-4 μm after 5 days) (data not shown). On the contrary, it was shown that gums were able to strongly decrease flocculation when adsorbed onto latex particles (D_h decreased from 1.68 at day one to 0.31 and 0.145 μm at day five when, respectively, 0.05% of *A. senegal* and 0.05% of *A. seyal* were adsorbed onto latex particles). However, even if gums stabilized latex particles, it was observed in time a large sedimentation of latex particles when dispersions were let at rest without agitation. Measurements of particles size in the latex dispersions supernatants gave however particles with $D_h > 1 \mu\text{m}$. The adsorbed layer thickness was therefore not able to be determined in screened conditions. These preliminary results were in disagreement with those recently reported by Gashua *et al.* (Gashua, et al., 2016) where authors determined, for the same latex particles samples, an adsorbed layer thickness of $\sim 40 \text{ nm}$ for *A. senegal* and $\sim 0.2 \text{ nm}$ for *A. seyal* in 0.5M NaNO_3 . Flocculation of latex particles in saline conditions, maybe modulated by the type of salt, could be at the origin of discrepancies in the latex dispersions behavior observed.

The adsorbed layer thickness values could be however determined in water, at pH 5.82, where no flocculation of free latex particles occurred in time, as a function of equilibration time. Figures 1a and 1b show the results of layer thickness values δ (nm) for gums adsorbed onto 0.1 μm carboxy or amidine latex particles after 15 days of equilibration. Data analyses highlighted the presence of one single peak after correlation function deconvolution confirming the presence of one single particle population assuming to represent gums adsorbed onto latex particles without aggregation or flocculation phenomenon.

It was first identified that the layer thicknesses were the highest ($\sim 100 \text{ nm}$ at equilibrium) in the case where both *A. senegal* macromolecules and latex particles were negatively charged, result very surprising considering the hypothetical repulsive electrostatic interactions occurring between GA macromolecules and latex particles. Similar behaviour was recently observed when GA adsorbed onto (negatively charged) gold surface (Davantes, et al., 2019). Lower layer thickness values ($\sim 50 \text{ nm}$ at equilibrium) were obtained when latex particles were positively charged. In the case of *A. seyal*, an invert behaviour was observed where the highest layer thicknesses ($\sim 50 \text{ nm}$) were obtained when *A. seyal* macromolecules adsorbed onto amidine latex particles, result in agreement, in this case, with the electrostatic complexation of negatively charged GA macromolecules onto the positively charged surface of latex particles.

A layer thickness δ ranging from 0.4 to $\sim 100 \text{ nm}$ was found depending on the type of gum and GA concentration, the lowest δ value being obtained for *A. seyal* (Figures 1a and 1b). An increase

of δ values with GA concentration was observed with a plateau reached only for *A. senegal* adsorbed onto carboxy or amidine latex particles at $C \sim 0.5\%$. By the contrary, a linear increase of δ values was observed for *A. seyal* with increasing GA concentration. The same behavior was noticed if protein content was reported instead of GA concentration on the x-axis (Figure 1b). In the case of negative latex particles, GA macromolecules adsorbed through the protein moiety and the presence of positive charges led to a decrease of entropy (and consequently an increase of enthalpy), compensated by a liberation of water molecules and/or counterions (entropy gain) and extension of the sugar blocks which kept highly hydrated. The electrostatic field of latex particles modifies the charge of some chemical groups and therefore facilitates GA adsorption. In the case of positive latex particles, the sugar blocks adsorb preferentially, leading to a greater compaction of adsorbed layers and therefore a thinner layer thickness. STEM images, obtained on hydrated samples, clearly revealed the presence of multiple flocs of bare latex particles of different sizes (Figure 2a) and the strong dissociation of latex flocs occurring after GA addition (Figures 2b, c, d, e). This strong dissociation was evidenced by DLS through the monomodal distribution of latex particles after GA adsorption always observed. However, the presence of dimers or multiplets in small quantity could not be neglected (Figure 2), as also observed recently, using centrifugal particle separation (CPS) and centrifugal field flow fractionation (CF3) experiments, for adsorption of antibodies onto latex particles (Contado, Mehn, Gilliland, & Calzolari, 2019). The presence of dimers and multiplets therefore overestimated the adsorbed layer thickness values determined by DLS. Bridging flocculation can not therefore be excluded in these experimental conditions, phenomenon that will lead also to overestimated layer thicknesses. The absence of two decays in the correlation functions simply means that flocs are weakly present by weight in the samples. In addition, as GA interacts with latex particles, flocculation by depletion is discarded as, in the theory, the key assumption is that there is no interaction between the particle and the polymer (Asakura & Oosawa, 1954). Another alternative explanation to explain the high layer thickness values measured in some conditions is that GA multilayers are formed onto the surface of latex particles as previously suggested by Gashua et al. (Gashua, et al., 2016). A4F measurements will confirm the formation of multilayers (see below). It is important to notice that multilayers formation does not prevent bridging flocculation to occur.

ζ potentials of latex particles after GA adsorption were also monitored and results were displayed on Figures 1c and 1d. It was clearly seen that adsorption of GA onto latex particles negatively (carboxy) or positively (amidine) charged led to ζ potential values close to GA alone with increasing GA concentration. At the highest GA concentration, latex particles reached ζ values of -23.7 and -11.6 mV for *A. senegal* and *A. seyal* adsorbed latex particles, respectively. A decrease of ζ values (less negative) with GA concentration was observed with a plateau reached for *A. senegal* and *A. seyal* adsorbed onto carboxy or amidine latex particles at a $C \sim 0.5\%$. This result showed that the strong adsorption of *A. senegal* and *A. seyal* onto negative latex particles could be due to the presence of positive charges coming from protein moiety, as suggested above.

3.2. Adsorbed layer structure : partial coverage, mono- and multilayers

A4F-MALLS was performed to characterize size (radius of gyration) and molecular weight of adsorbed GA latex particles. **Dilution of the samples was necessary in order to avoid saturation of LS and RI detectors.** One example of fractograms obtained on bare latex and GA adsorbed latex particles is given on Figure S1 (supplementary information). From these data, it was possible to calculate the different parameters available from this method: radius of

gyration, molecular weight and polydispersity index (R_g , M_w , M_w/M_n) (Table 2). Using the following equation, it was also possible to calculate the number of GA macromolecules adsorbed onto carboxy and amidine latex particles:

$$\text{Number of adsorbed GA} = \frac{M_w^{\text{latex+GA}} - M_w^{\text{latex}}}{M_w^{\text{GA}}} \quad (4)$$

with M_w of *A. senegal* and *seyal* of $6.86 \cdot 10^5$ and $8.31 \cdot 10^5$ g.mol⁻¹, respectively. **The known number of adsorbed GA per latex particle allowed the calculation of the surface coverage (Table 2).**

The number of adsorbed GA macromolecules was the highest in the case of *A. senegal* adsorbed onto positively charged amidine latex particles, in agreement with an electrostatic complexation between the surface of latex particles and GA macromolecules (Table 2). Increasing GA concentration from 0.00095 to 0.095% (w/v) led to a number of adsorbed GA macromolecules from 1059 to 2158. From the calculations of surface coverages (Table 2), it was concluded that partial coverage, monolayer or multilayer, depending on GA concentration, formed the structure of the GA layer adsorbed onto carboxy latex particles while multilayer always be effective for GA layer adsorbed onto amidine latex particles.

The relationship between the adsorbed layer thickness δ (nm) as a function of the number of adsorbed GA macromolecules is depicted on Figure 3a. A first remark was that the thickness increased with the number of adsorbed GA macromolecules except for *A. seyal* adsorbed onto amidine latex where the layer thickness decreased with the increase of adsorbed GA macromolecules.. This is certainly due to rearrangement of AGPs during or after adsorption, as it was previously seen for fibrinogen adsorption with a side-on and/or end-on mechanism depending on pH (Bratek-Skicki, Zeliszewska, & Ruso, 2016). In particular, for *A. senegal* adsorbed onto carboxy latex particles, the layer thickness was the highest while the number of GA adsorbed was the lowest (Figure 3a). By the contrary, for *A. senegal* adsorbed onto amidine latex particles, the layer thickness was the lowest while the number of GA adsorbed was the highest. However, it was interesting to note that while the number of adsorbed GA macromolecules increased, the layer thickness kept rather constant and reached a pseudo-plateau for the highest values except for *A. seyal* adsorbed onto amidine latex particles where the layer thickness decreased while the number of GA adsorbed increased. This last result simply means that, with increasing GA concentration, a compaction of the adsorbed layer occur with or without GA conformational changes associated.. R_g remained constant in the case of adsorbed GA (*senegal* or *seyal*) onto carboxy latex particles, probably due to the maximum of packing due to repulsions between latex particles and GA of same sign. These results reinforce the hypothesis that the mechanism of adsorption would differ depending on the charge of latex particles due to the duality of charges on GA macromolecules. The differences between the two gums come partly from the less positive and negative charges on *A. seyal* (Table 1, ζ potential value twice higher for *A. senegal*).

The relationship between the ratio R_g/R_h of GA adsorbed onto latex particles was depicted on Figure 3b. While R_g/R_h decreased with the increase of the number of adsorbed GA onto latex carboxy particles, meaning that compaction of particles increased with the increase of layer thickness, the relationship for both gums with amidine latex particles was much more complicated. The ratio for *A. senegal* adsorbed onto amidine latex particles increased then abruptly decreased, meaning that particles first swelled before to be strongly compacted. This phenomenon could be due to rearrangements/interpenetration of GA macromolecules onto the latex surface associated or not to changes of adsorbed layer hydration giving rise to

swelling/compaction phenomena. It was therefore found that swelling occurred when gums adsorbed onto amino latex particles were dried and rehydrated (data not shown). An increase of 106% and 285% of the adsorbed layer after drying and rehydration was found for *A. senegal* and *A. seyal*, respectively. In the case of *A. seyal* adsorbed onto amidine latex particles, the behaviour was rather complex (Figure 3b). The ratio R_g/R_h slightly decreased with the increase of number of GA adsorbed then abruptly increased while the number of GA adsorbed increased. It is well known that water moderates protein adsorption to any surface through more or less intense dehydration of adsorbing protein molecules (Vogler, 2012). As GA contains polypeptidic backbone, the competition between water and polypeptidic backbone for the latex surface could induce complex behaviour of the adsorption process, as revealed by the complex relationship observed between the ratio R_g/R_h and the layer thickness.

3.3. Evolution of adsorbed GA layer with pH: electrostatics vs hydrophobic effect

As electrostatic interactions play a crucial role in the adsorption properties of GA onto latex particles, layer thicknesses and ζ potentials of GA adsorbed onto carboxy and amidine latex particles were measured over time as a function of pH ranging from 3 to 8. Values obtained after 12 or 14 days of equilibration are depicted on Figure 4. ζ -potential values of bare latex and gum alone were also added for comparison. A marked effect of adsorption capacity was noticed with decreasing pH from 8 to 3 with a thickness layer varying from 21.5 to 112.1 nm for *A. senegal* and from 6 to 43.1 nm for *A. seyal*. The most pronounced effect was noticed at pH 3 in conditions where *A. senegal* and *A. seyal* were slightly negatively charged (electrophoretic mobility of -12.5 and -6.8 mV for *A. senegal* and *A. seyal*, respectively) and more hydrophobic, leading to a greater adsorption. The duality of positive and negative charges on GA macromolecules coupled to hydrophobic effect leading to conformational changes is at the origin of the abnormal enhanced GA adsorption at pH 3. Some authors argued in favour of heterogenous charge distribution on protein molecules to explain this phenomenon (Wasilewska & Adamczyk, 2011).

As observed previously, in the case of amidine latex particles, the thickness of *A. senegal* layer was lower than for carboxy latex particles while the inverse applied for *A. seyal* (Figure 4). These lower thicknesses were however in favour of higher GA content adsorbed onto latex particles (Table 2), highlighting the great compaction of the layer maybe due to the higher flexibility of sugar blocks compare to the protein moiety. It was therefore surprising to notice that in conditions of attractive electrostatic interactions between negative *A. senegal* and positive amidine latex particles, the adsorption layer thickness was smaller whatever the pH used. A possible different organization of AGPs with a « stretching » or « flattening » of macromolecules would occur when the repulsive potential is greater, leading to a higher layer thickness. The « flattening » of soft colloids such as microgels was recently demonstrated where authors provided strong numerical evidence that microgels adsorbed at an interface behave like 2D elastic particles, with a « fried-egg » shape, in stark contrast to what was found in bulk conditions (Camerin, et al., 2020). Moreover, softness provides the particle with an additional degree of freedom to get reshaped instead of deforming the interface (Mehraban, Snoeijer, & Harting, 2020).

ζ potentials confirmed the adsorption of GA macromolecules onto carboxy or amidine latex particles as ζ potential values of GA adsorbed onto latex particles were intermediate between those of bare latex and gum alone after 12 or 14 days of equilibration (Figure 4).

3.4. Evolution of adsorbed layer with protein content: fair correlation

As described in the Introduction, the protein content in AGPs from GA influence the adsorption behavior on latex particles. Adsorption layer thicknesses were then probed on both *A. seyal* and *A. senegal* and its molecular fractions HIC-FI, HIC-FII and HIC-FIII, on two types of negatively charged latex particles, latex of 0.1 μm (ζ potential -43.2 mV) and latex amino of 0.5 μm (ζ potential -19.6 mV) (Figure 5a, 5b, Table 3). **Latex particles of 0.5 μm was highly stable in time with no sedimentation due to gravity.** These two type of latex particles were therefore chosen to highlight adsorption process depending on the size and the magnitude of charge of latex particles. The highest δ value of 231 ± 6.3 nm was obtained for HIC-FII at 0.05% after 14 days of adsorption (Figure 5a). In addition, it was interesting to note that a concentration as low as 0.003% (30 ppm) (HIC-FIII) was able to give an adsorbed layer thickness of 7.6 ± 0.7 nm. This result was however in agreement with those reported by Bergenståhl *et al.* where authors revealed steric stabilization of latex particles for several gums included gum arabic already at low concentrations (ppm range) (Bergensthål, Fogler, & Stenius, 1986). A fair agreement was found between the layer thickness and the protein content, the highest layer thickness being closely related to the highest protein content (Figure 5c, Table 3). The most efficient AGPs to stabilize latex dispersions would be therefore FIII molecular fraction from *A. senegal* considering the layer thickness value (7.6 nm) obtained for a very low FIII concentration (0.003%), fraction having therefore the highest protein content. However, the differences observed in layer thickness values for very similar protein content would suggest that the protein content would not be the unique parameter to take into account to understand the adsorption behaviour of gums and molecular fractions at solid-liquid interfaces. **It was therefore recently demonstrated that the high molecular weight AGP fraction was also an important biochemical parameter involved in the adsorption process (Davantès, Nigen, Sanchez, & Renard, 2021).** In addition, it was found that decreasing ζ potential of latex particles, even if the size of latex particles was bigger (0.5 vs 0.1 μm), led to an adsorbed layer thickness two to three-fold higher, meaning that the lowering of repulsive electrostatic interactions had a substantial effect on the adsorption properties of *A. senegal* and *A. seyal* gums (Figure 5, Table 3).

3.5. Structure of adsorbed layer using microscopy: presence of aggregates

The structure of GA and its fractions adsorbed layers onto latex particles was first probed using transmission electron microscopy (Figure S2, a-f). It was clearly identified that bare latex particles were present as core-shell or matricial structure (yellow arrows, Figure S2). This first observation would imply that false interpretations on the structure of GA adsorbed layer onto latex particles could be done using microscopy. Indeed, the other images on *A. senegal*, *A. seyal*, HIC fractions adsorbed onto latex particles did not allow the clear identification of the adsorbed layers but rather reveal diffuse structures around particles. The « black » layers identified at the surface of GA adsorbed latex particles were also present on bare latex particles. These results did not corroborate those obtained by Gashua *et al.* (Gashua, et al., 2016) where authors confirmed that the GA molecules had formed a distinct, thick adsorbed layer surrounding latex particles. Our present observations did not however revealed clear and distinct layers when images were compared with those obtained from bare latex particles.

Nor AFM nor SEM images were also able to clearly identify a GA layer thickness onto latex particles probably for sample preparation reasons (in particular dehydration) before microscopy observations (Figure S2).

NanoInfraRed spectroscopy was used to try to evidence the GA gums adsorbed onto latex particles. In the spectroscopic mode, the different spectra were obtained for the bulk material (latex and gums) and for the GA functionalized latex particles (Figure 6). For the nanoIR spectra

and to emphasize the differences between the samples, all the spectra were normalized by fixing the band at 1493 cm^{-1} characteristic of latex particles at 1 (Figure 6B). Similar spectra were obtained on *A. senegal* gum using classical IR and nanoIR (compare Figure 6A with Figure 6B). Spectra were also similar for bare latex particles whatever the method used. As expected, the band at 1493 cm^{-1} characteristic of the latex is detected for the bare latex particles and a large band around 1650 cm^{-1} characteristic of the GA is visible for the bulk GA. When acquiring spectra on the functionalized latex particles, the NanoIR spectra were similar whatever the gum used. The bands characteristics of latex at 1493 cm^{-1} and gums at 1654 cm^{-1} were clearly identified, while the latter are not visible on the bare latex particles. The sum of individual latex and GA spectra were close to that of the adsorbed gum onto latex particle spectra (data not shown). A decrease of band intensities at $\sim 1730\text{ cm}^{-1}$ was noticed after GA adsorption, characteristic of GA covering the surface of latex beads. On the contrary, an increase of band intensities at $\sim 1380\text{ cm}^{-1}$ was noticed after GA adsorption. The shoulder identified at 1654 cm^{-1} , characteristic of GA, shifted towards higher frequencies after GA adsorption (1659 cm^{-1} for *A. seyal* and 1661 cm^{-1} for *A. senegal*). These shifts were ascribed to some conformational changes of GA after adsorption or a decrease of hydrogen bond energy due to the adsorption-induced dehydration process.

By looking at the nanoIR spectra (Figure 6B), between bare latex and GA adsorbed latex spectra, the band around 1650 cm^{-1} was observed with a strong intensity for the GA while very weak for the bare latex particle. Thus, this wavenumber was chosen to perform IR mapping on GA adsorbed latex particles (). The first images were performed with a high density of latex particles to ensure to detect sufficient signal. Topographical images of bare latex particles and *A. senegal* and *A. seyal* adsorbed latex particles were displayed on Figures 7A (a), 7B (d) and 7C (i) while two-dimensional IR mapping were shown on Figures 7A (b), 7B (e), 7C (j)). For the bare latex particles, the IR intensity mapping exhibit a very weak signal (blue color on the scale bar) confirming the absence of an IR absorption for this wavenumber. On the contrary, for both *A. senegal* and *A. seyal* gums adsorbed onto latex particles a clear signal (yellow in the scale bar) was detected meaning that GA was present onto the surface of latex beads and thus confirming the efficient adsorption. On these images, a few blue spots could be detected (see arrow on the figure) which correspond to the absence of particles on the surface as seen on the topographical images. However, the images for *A. seyal* adsorbed latex particles were more blurred, meaning certainly that *A. seyal* gum spread over latex particles and solid surfaces used to probe images. Then, to be sure of the GA adsorption on the latex particles, isolated particles were then studied after dilution of the initial solutions as observed in the topographical images (Figure 7). Whatever the gum used, IR mapping (obtained in the same conditions as previously) clearly showed that GA was only detected at the surface of latex particles (red signal corresponding to high IR intensities) while almost no gum was detected on the substrate without particles (blue signal corresponding to a very weak IR absorption). This result clearly evidenced the successful functionalization of the particles using chemical features and imaging.

, Similar NanoIR experiments were performed using molecular fractions (FI, FII, and FIII) adsorbed onto latex particles (Figure 8). From nanoIR spectroscopy, four spectral regions were identified as being ascribed to the adsorption and denoted « adsorption specific » in the Figure. The band intensity changes were essentially due to the adsorption of molecular fractions onto latex particles, leading to a decrease of band intensity of chemical residues absorption specific to latex particles. In particular, the strong band at 1599 cm^{-1} (carboxylate group) strongly decreased after GA adsorption. On the contrary, bands specific to molecular fractions were identified in the nanoIR spectra, where latex absorption was negligible ($\sim 1650\text{ cm}^{-1}$ and $\sim 1350\text{ cm}^{-1}$). In particular, vibrations of amide I and amide II bands are located near 1650 and 1550 cm^{-1} .

¹, respectively. When trying to perform imaging, for the latex particles functionalized with the FI fraction, AFM images revealed the presence of elongated crystals leading to a layer covering the substrate with only some particles visible (Figure 8A (b)), which was not the case when using whole gum. For FII and FIII functionalized latex particles, no such issue was observed as seen in the topographical images and both samples behave as functionalized latex + *A. senegal* with a mapping at 1654 cm⁻¹ clearly revealing the functionalization of latex beads by FII or FIII macromolecules. Rough surfaces of FII and FIII functionalized latex particles were observed by AFM and SEM (Figure S2). These rough surfaces came from the presence of aggregates adsorbed onto the surface, these aggregates being yet present in solution or being formed during adsorption.

3.6. Conformational changes associated to GA adsorption onto latex particles: weak but present

Adsorption of proteins onto solid-liquid or liquid-liquid interfaces is often accompanied by conformational changes (Aberkane, et al., 2012; Dickinson, 1988, 2003, 2008; Dickinson, et al., 1988; Firkowska-Boden, Helbing, Dauben, Pieper, & Jandt, 2020; Guo, Zhang, Chu, Jiang, & Li, 2020; Jia, Zhao, Lin, & Su, 2020; Ma, Ferhan, Jackman, & Cho, 2020; Padala, Williams, & Phillips, 2009; Tian, et al., 2020; Trindade, et al., 2008; S. N. Wang, et al., 2020; Zhai, Day, Aguilar, & Wooster, 2013). Using fluorescence or infrared spectroscopy, authors were able to probe conformational changes of proteins in particular at liquid-solid interfaces in emulsions (Audebrand, Ropers, & Riaublanc, 2013; Castelain & Genot, 1994, 1996; Rampon, et al., 2004). It was previously demonstrated that the surface activity of globular proteins was intimately related to their molecular compressibility and their susceptibility to conformational changes at the interface (Razumovsky & Damodaran, 1999). Furthermore, some authors claimed that protein adsorption is primarily controlled by water/surface interactions (Parhi, Golas, Barnthip, Noh, & Vogler, 2009).

In the present work, fluorescence spectroscopy was used in order to probe possible conformational changes of GA after adsorption onto latex particles. In addition, time-correlated fluorescence spectroscopy was applied in order to probe at the molecular level fluorescence decay of bare latex and GA adsorbed onto latex particles. From steady-state fluorescence measurements, the strong fluorescence emission of latex particles in the same wavelength range as GA macromolecules limited real conformational changes to be probed particularly at low GA concentration. All the results obtained from steady-state fluorescence clearly revealed no conformational changes of GA after adsorption onto latex particles (see Supporting Information).

However, from lifetime measurements (see Supporting Information, Table S1), it was concluded that some molecular changes, in the vicinity of aromatic residues, with or without overall conformational changes associated when GA adsorbed at the surface of latex particles at low GA concentration, occurred. This result was in agreement with the band shift observed by nanoIR after GA adsorption.

4. Discussion

4.1 Electrostatic and hydrophobic effect related to protein moiety and leading to conformational changes drive the adsorption process

Previous study on the adsorption of GA onto flat gold surface revealed first that 150 ppm and 500 ppm of *A. senegal* and *A. seyal*, respectively, fully covered the gold surface (1 cm²) and second that surface density ranged from 0.92 to 3.83 mg m⁻² using SPR (i.e., “dry” mass) and

from 1.16 to 19.07 mg m⁻² using QCM-D (wet mass). In addition, and very surprisingly, the mass adsorbed was the highest at pH 7.0 in conditions of strong electrostatic repulsions between the gold substrate (slightly negative) and AGPs (negative), highlighting the contribution of other interactions than electrostatics involved in the adsorption process (Davantes, et al., 2019).

By comparing the adsorption behavior of both gums with amidine and carboxy latex particles, it was noticed that the amidine/carboxy layer thickness ratio was lower than 1 in the case of *A. senegal* at $C > \sim 0.01$ % while this ratio was found to be higher than 1 in the other cases (Figure S6 (a)). Whatever the GA concentration used, the ratio was always higher in the case of *A. seyal* adsorbed onto latex particles, highlighting the importance of the charge distribution and/or conformation in the better adsorption capacity of *A. seyal*. It was also noticed that the ratio decreased with increasing GA concentration to reach a value close to 0.5 at $C = 1$ %, highlighting the absence of effect of electrostatic interactions, between both negatively charged GA and latex particles or positively charged latex particles and negatively charged GA macromolecules, at high GA concentration. At fixed GA concentration (0.0475% or 475 ppm), the effect of amidine/carboxy layer ratio was again higher in the case of *A. seyal* adsorbed onto latex particles whatever the pH used (Figure S6 (b)). A ratio lower than 1 was always observed in the case of *A. senegal* whatever the pH used. These results would mean that while *A. seyal* behave classically with latex particles of opposite charge, with a strong adsorption capacity whatever the C and pH used (δ ratio always higher than 1), this was not the case for *A. senegal* where higher adsorption occurred at low GA concentration (i.e. for $C < 0.01$ %, ratio > 1) and lower adsorption occurred at higher concentration and at fixed concentration whatever the pH used (Figure S6 (b)). Surprisingly, the δ ratio decreased with the increase of negative charges on GA (i.e. by increasing pH), result in apparent contradiction with the increase of attractive electrostatic interactions that should occur between **negatively charged** GA and **positively charged** amidine latex particles. This behavior would question about the mechanism involved in the adsorption of both gums whatever the chemical nature (gold, amidine or carboxy latex) and the geometry (flat or curved) of the surface. The presence of positively charged amino acids in the **protein moiety** of GA macromolecules could be the driving force leading to this anomalous adsorption phenomenon. These results were however in agreement with the adsorption of negatively charged fibrinogen onto positively charged latex particles where authors explained that it was the result of the side-on adsorption of fibrinogen molecules with their negatively charged core attached to the positively charged latex surface (Bratek-Skicki, Zeliszewska, & Adamczyk, 2013; Bratek-Skicki, Zeliszewska, Adamczyk, & Ciesla, 2013; Bratek-Skicki, et al., 2016; Zeliszewska, Bratek-Skicki, Adamczyk, & Ciesla, 2014). In addition, other authors identified that fibrinogen became more denatured on small particles having a higher surface curvature (Roach, Farrar, & Perry, 2005, 2006). Other study confirmed what was obtained on fibrinogen where BSA was found to adsorb in the « side-on » position and became flattened due to exposure to the oppositely charged surface (Cowsill, et al., 2011). Authors also identified a layer thickness ranging from 3 to 8 nm depending on BSA concentration. Flattened « wetted » individual BSA were therefore present at low surface coverage while compact individual BSA were present at high surface coverage. In the present study, it was identified that conformational changes and/or flexibility of AGPs occurred after adsorption onto latex particles at low GA concentration (see fluorescence lifetimes results) while compaction of AGPs leading to multilayer structures was formed at higher GA concentration (see Table 2).

Hydrophobic effect leading to conformational changes and accessibility of the protein moiety or the amphipathic β -1,3 galactan structure should be considered to understand gum adsorption phenomena. It should be pointed out that GA self-aggregation can occur between negatively

charged sugar blocks and positively charged amino acids of protein moiety, this self-aggregation having consequences on GA adsorption. On the molecular basis, fluorescence lifetime measurements and nanoIR mapping partly revealed some slight changes due to GA adsorption onto latex particles. The exploration of structural changes during adsorption was previously monitored through QCM-D experiments on flat gold surfaces but the method was not able to discriminate between conformational changes and/or hydration content changes (Davantes, et al., 2019).

To qualitatively summarize the adsorption properties of GA onto latex particles, based on results on Figure 1 and Figure 3, it was confirmed that the adsorption was the highest in terms of layer thickness when GA and latex particles were both negatively charged (Table 2), highlighting the presence of interactions other than electrostatic in the adsorption process. Previous literature identified that the charge density of a labile polyelectrolyte was regulated by the electrical potential of latex surfaces, facilitating therefore adsorption between polysaccharide and latex particles of the same sign (Zhang, Pelton, Ketelson, & Meadows, 2011). Authors also argued that small ions may contribute to the adsorption when like charged protein and particle are mixed together, the redistribution of ions having a consequence on the water molecules being released during adsorption (de Vos & Lindhoud, 2019).

It was assumed, in line with adsorption studies on flat gold surfaces, that the adsorbed layers were more or less hydrated depending on the charge of latex particles and the nature of GA (Table S1). Interestingly, the highest hydrated layer was obtained in the case where the highest electrostatic repulsions occurred (latex carboxy – *A. senegal*). Two explanations are given in literature to explain the adsorption of like charged (negative) protein and particle or surface (de Vos, et al., 2019): a chemical explanation as the protein contains a reasonable number of basic amino acids and adsorption arises from electrostatic attraction between this positively charged patch and the negatively charged latex surface or a physical explanation as the protein could change its conformation such that the hydrophobic residues which in solution are mainly buried could be partially exposed upon adsorption (i.e. hydrophobic effect) and interact with the surface. From these explanations, and considering that some conformational changes of GA after adsorption were probed by fluorescence lifetime studies and nanoIR mapping, both specific electrostatic attractions between positive charges of the GA protein moiety and negatively charged latex particles and related conformational changes were important for the adsorption in conditions of strong repulsive interaction coupled with a high hydration level, as evidenced by Davantes *et al.* on gold surfaces (Davantes, et al., 2019). Some authors explained protein adsorption to similarly charged surfaces by charge inversion of proteins through charge regulation (Boubeta, Soler-Illia, & Tagliacuzzi, 2018; de Vos, et al., 2019; Hartvig, van de Weert, Ostergaard, Jorgensen, & Jensen, 2011; Lund, Akesson, & Jonsson, 2005). Adsorption can be enhanced by several kT due to changes of protonation state when a protein approaches a charged surface (Lund, et al., 2005). Other authors identified attractive interactions between two negatively charged polysaccharides through the protein moieties of GA (Padala, et al., 2009; Sabet, et al., 2021).

On the contrary, the attractive potential between positively charged latex particles and negatively charged GA did not lead to a strong adsorption nor a high layer thickness, even if the number of GA macromolecules adsorbed was the highest for *A. senegal* adsorbed onto latex amidine (Table 2). The number of adsorbed GA macromolecules therefore differed depending on the positive or negative surface of latex particles. This result would mean that either polysaccharide blocks or polypeptide backbone would be the first moieties to adsorb onto

charged latex particles and that structural rearrangements would lead to different levels of hydration of the adsorbed layers. Structural flexibility of GA will orient polysaccharide blocks and protein moiety towards a charged surface to maximize electrostatic attraction. As AGPs from *A. senegal* and *A. seyal* have different structural compressibilities (V. M. Tamayo, et al., 2018), the maximization of attraction would not be always fulfilled. It should be pointed out that the comparison of adsorption properties of AGPs with proteins should therefore be taken with high cautious due to the high molar mass of AGPs compare to proteins.

4.2. Adsorbed layers are inhomogeneous, homogeneous or aggregated depending on GA concentration and the chemical nature of GA

Besides the reasonable correlation found between layer thickness and protein content (Figure 1b), with an increase of δ with protein content until a plateau was reached, we may wonder whether monolayer or multilayer adsorbed gums and molecular fractions were present onto the surface of latex particles. From A4F results, it was found, from surface coverage calculations, that the layer structure for GA adsorbed onto carboxy latex particles was partially covered, formed a monolayer or a multilayer with increasing GA concentration (Table 2). In addition, a multilayer structure was formed for GA adsorbed onto amidine latex particles. This gave three regimes for the layer structure: partial coverage for $\delta < 2$ nm, a monolayer for $2 < \delta \leq 10$ nm and a multilayer for $\delta \geq 10$ nm.

From the layer thickness values of gums and molecular fractions reported in Table 3, it could be concluded that the layer structure was partially covered for *A. seyal* at 0.01%, formed a monolayer for *A. seyal* at 0.05%, HIC-FI and HIC-FIII at 0.003% while a multilayer was formed for *A. senegal*, HIC-FII and HIC-FIII at 0.01%. However, differences in structure of gums and molecular fractions at solid interfaces compare to bulk could lead to misinterpretations in the type of layer structure. It is well known that gums easily self-associate in bulk and in particular in water (Dror, Cohen, & Yerushalmi-Rozen, 2006; Renard, Garnier, Lapp, Schmitt, & Sanchez, 2012, 2013; Renard, Lavenant-Gourgeon, Lapp, Nigen, & Sanchez, 2014; Sanchez, et al., 2008; V.M. Tamayo, 2018; Q. Wang, Burchard, Cui, Huang, & Phillips, 2008) but there is no experimental evidence today on the same phenomenon occurring at solid interfaces. The presence of rough surfaces onto latex particles after GA adsorption identified by microscopy (see Figure S2) was in relation to the GA self-association in water. It could be easily supposed for instance that the highest δ values found for HIC-FII ($\delta = 230.8$ nm) and HIC-FIII ($\delta = 178.0$ nm) at 0.05 and 0.01% concentration, respectively, could be related to aggregates formed in bulk and adsorbed then onto solid surfaces, as demonstrated on GA, HIC-FII and HIC-FIII where aggregates of 150, 150 and 125 nm, respectively, were evidenced in solution in water (V.M. Tamayo, 2018). In addition, Wang et al. showed that R_g of GA ranged from 20 nm at $C = 0.0413$ g/L (i.e. 41.3 ppm) to 50 nm at $C = 5.21$ g/L (i.e. 5210 ppm), the growth of GA dimension with concentration being ascribed to self-association (Q. Wang, et al., 2008). **Alternatively, bridging flocculation was certainly present in these samples**, in accordance with the experimental evidence of flocculation occurring depending on gum arabic concentration reported by Garti et al. and Gashua et al. (Garti & Reichman, 1993; Gashua, et al., 2016).

The present study highlighted the importance of GA addition to the important decrease of latex particles flocculation (Figure 2). STEM images clearly unraveled the important deflocculation process occurring when gums or molecular fractions were adsorbed onto latex particles. Further studies should therefore be performed to reveal the self-association of adsorbed gums at

interfaces and in particular the potential conformational changes and structural rearrangements occurring during adsorption.

Results displayed on Figure 5b and Table 3 dealt with the adsorption properties of *A. senegal* and *A. seyal* gums onto amino latex particles of 0.5 μm size in water. Again, a progressive increase of the adsorption layer thickness in time was noticed until a (pseudo)-plateau value was reached after 11 days of equilibration time. A fair correlation was again found between the adsorption layer thickness δ and the protein content in agreement with the results obtained for latex particles of 0.1 μm size. The δ value therefore increased with the increase of GA concentration. However, the adsorption layer thickness δ was always higher for gums adsorbed onto 0.5 μm amino latex particles compare to 0.1 μm latex particles. A $\delta_{\text{amino latex}} / \delta_{\text{latex}}$ ratio ranging from 2.3 to 3.0 was therefore calculated (Table 3), highlighting the substantial improvement of adsorption efficiency of gums when adsorbed onto 0.5 μm amino latex particles. Not only size but also the magnitude of charge had an impact on the adsorption of GA.

By addition of gums (*A. senegal* or *A. seyal*), the adsorption onto amino latex particles induced a decrease of the negative ζ potential values, when *A. seyal* was adsorbed, ranging from -19.6 to -11.9 mV with increasing *A. seyal* gum concentration, and a slight increase when *A. senegal* was adsorbed, ranging from -19.6 to -22.9 mV (Table 3). It was previously checked that gums alone (C = 1%, w/w) displayed a negative ξ value when dispersed in water at pH 6 (or 7) with ξ value of -25.2 mV for *A. senegal* and -11.6 mV for *A. seyal* (Table 1). Interestingly, it was noticed that the ζ potential value decreased (*i.e.* ζ value more negative) when the layer thickness of GA-amino latex particles was low, *i.e.* $\zeta = -12.1$ or -11.9 mV and $\delta \sim 10.4$ or 15.3 nm for *A. seyal* while $\zeta \sim -21.7$ or -22.9 mV and $\delta = 36.5$ or 71.0 nm for *A. senegal* (Table 3). The average number of charges ratio for amino latex / GA were of 8.2 and 22.5 for *A. senegal* and *A. seyal*, respectively (Table 1). The higher excess of negative charges in the case of amino latex – *A. seyal* dispersions led to a decrease of the layer thickness, in agreement with the increase of repulsive potential between GA macromolecules and the surface.

Results of ζ potential value after adsorption of gums or molecular fractions onto latex particles of 0.1 μm diameter were more complex (Table 3). In particular, there was no clear relationship between the evolution of the ζ potential values and the layer thickness while a clearer relationship existed between the layer thickness and the protein content. This result would question again about the possible formation of multilayer formation and the absence of correlation between the adsorbed layer thicknesses and the ζ potential values. This question was partly solved through A4F measurements where it was shown that monolayer and multilayer films of GA adsorbed onto latex particles existed depending on GA concentration (Table 2). However, it should be pointed out that the highest GA content adsorbed in terms of number of macromolecules was obtained with amidine latex particles. Hydration forces due to the high solvation of GA layers **should** also play a crucial role in the adsorption process. From A4F experiments, it was also clearly demonstrated that compaction of adsorbed layers occurred with the increase of the number of adsorbed GA onto latex particles (Figure 3b). This phenomenon was particularly true with carboxy latex particles while swelling and compaction of the adsorbed layers occurred when GA was adsorbed onto amidine latex particles. A summary of adsorption properties of *A. senegal* and *A. seyal* gums onto latex particles was given in Table 5.

5. Conclusions

Adsorption of GA onto latex particles revealed a complex mechanism of adsorption where the highest adsorption was often observed when both GA and latex particles were negatively

charged. This result confirmed previous results obtained on the adsorption of GA onto flat gold surfaces, highlighting the contribution of other interactions involved in the adsorption process. However, electrostatic interactions played a crucial role in the adsorption process where the mechanism would be controlled by the electrostatics of GA and their modification by the electrostatic potential of latex particles. The importance of positive charges coming from amino acids of the **protein moiety** seems evident, and **highlighted** mechanisms where either the **protein moiety through hydrophobic effect** or the sugars blocks should adsorb. This mechanism produced differences of behaviour due to viscoelastic properties of adsorbed layers, differences of hydration due to differences of polarity of AGPs. The major role of electrostatics in the adsorption process had as a consequence water release from the adsorbed layers and important gain in entropy. Hydration forces due to the high **solvation** of GA layers should therefore play a crucial role in the adsorption process. A reasonable agreement was found between protein content and adsorption layer thickness of GA adsorbed layer, with the evidence of the formation of partial coverage, monolayer and multilayer films depending on GA concentration. Structural changes induced by GA adsorption onto latex particles were probed using fluorescence lifetime measurements and nanoIR mapping. HIC fractions adsorbed onto latex particles did not allow the clear identification of the adsorbed layers but rather reveal diffuse structures around particles.

The results of this **study** highlighted that GA surface adsorption process would depend not only on the protein moiety but also on other parameters such as the structural accessibility, the molecular weight distribution, the AGPs flexibility allowing structural rearrangements on the surface and spreading in order to form a viscoelastic film adsorbed onto latex particles. Future work should be focused on the real time adsorption process through spectroscopic techniques on hydrated latex dispersions in order to probe structural changes during GA adsorption.

Acknowledgments

The authors would like to express their gratitude to the French Alland & Robert company for a financial sponsorship of one co-author (A. Davantès). We would like also to thank J. Davy for the samples preparation and SEM observations. We are grateful to N. Stephant for SEM facilities and expertise at IMN (Nantes, France). We acknowledge S. Durand for IR characterization of latex and gums and N.B. Bercu for technical assistance with the nanoIR.

References

- Aberkane, L., Jasniewski, J., Gaiani, C., Hussain, R., Scher, J., & Sanchez, C. (2012). Structuration mechanism of beta-lactoglobulin - acacia gum assemblies in presence of quercetin. *Food Hydrocolloids*, 29(1), 9-20.
- Adamson, A. W., & Gast, A. P. (1997). *Physical-Chemistry of Surfaces* (6th ed.): John Wiley & sons, USA.
- Alftren, J., Penarrieta, J. M., Bergenstahl, B., & Nilsson, L. (2012). Comparison of molecular and emulsifying properties of gum arabic and mesquite gum using asymmetrical flow field-flow fractionation. *Food Hydrocolloids*, 26(1), 54-62.
- Aphibanthammakit, C., Barbar, R., Nigen, M., Sanchez, C., & Chalier, P. (2020). Emulsifying properties of Acacia senegal gum: Impact of high molar mass protein-rich AGPs. *Food Chemistry-X*, 6.
- Aphibanthammakit, C., Nigen, M., Gaucel, S., Sanchez, C., & Chalier, P. (2018). Surface properties of Acacia senegal vs Acacia seyal films and impact on specific functionalities. *Food Hydrocolloids*, 82, 519-533.
- Asakura, S., & Oosawa, F. (1954). On Interaction between Two Bodies Immersed in a Solution of Macromolecules. *The Journal of Chemical Physics*, 22(7).

- Atgie, M., Chenneviere, A., Masbernat, O., & Roger, K. (2019). Emulsions Stabilized by Gum Arabic: How Diversity and Interfacial Networking Lead to Metastability. *Langmuir*, 35(45), 14553-14565.
- Atgie, M., Masbernat, O., & Roger, K. (2019). Emulsions Stabilized by Gum Arabic: Composition and Packing within Interfacial Films. *Langmuir*, 35(4), 962-972.
- Audebrand, M., Ropers, M. H., & Riaublanc, A. (2013). Disappearance of intermolecular beta-sheets upon adsorption of beta-lactoglobulin aggregates at the oil-water interfaces of emulsions. *Food Hydrocolloids*, 33(2), 178-185.
- Balantrapu, K., & Goia, D. V. (2009). Silver nanoparticles for printable electronics and biological applications. *Journal of Materials Research*, 24(9), 2828-2836.
- Bergenthâl, B., Fogler, S., & Stenius, P. (1986). The influence of gums on the stability of dispersions. In G. O. Phillips, D. J. Wedlock & P. A. Williams (Eds.), *Gums and Stabilisers for the Food Industry* (IRL Press ed., Vol. 3, pp. 285-293). Oxford.
- Boubeta, F. M., Soler-Illia, G., & Tagliacuci, M. (2018). Electrostatically Driven Protein Adsorption: Charge Patches versus Charge Regulation. *Langmuir*, 34(51), 15727-15738.
- Bratek-Skicki, A., Zeliszewska, P., & Adamczyk, Z. (2013). Tuning conformations of fibrinogen monolayers on latex particles by pH of adsorption. *Colloids and Surfaces B-Biointerfaces*, 103, 482-488.
- Bratek-Skicki, A., Zeliszewska, P., Adamczyk, Z., & Ciesla, M. (2013). Human Fibrinogen Monolayers on Latex Particles: Role of Ionic Strength. *Langmuir*, 29(11), 3700-3710.
- Bratek-Skicki, A., Zeliszewska, P., & Ruso, J. M. (2016). Fibrinogen: a journey into biotechnology. *Soft Matter*, 12(42), 8639-8653.
- Buffo, R. A., & Reineccius, G. A. (2000). Beverage emulsions and the utilization of gum acacia as emulsifier/stabilizer. *Perfumer & Flavorist*, 25, 24-44.
- Camerin, F., Gnan, N., Ruiz-Franco, J., Ninarello, A., Rovigatti, L., & Zaccarelli, E. (2020). Microgels at Interfaces Behave as 2D Elastic Particles Featuring Reentrant Dynamics. *Physical Review X*, 10(3).
- Castelain, C., & Genot, C. (1994). Conformational-changes of bovine serum-albumin upon its adsorption in dodecane-in-water emulsions as revealed by front-face steady-state fluorescence. *Biochimica Et Biophysica Acta-General Subjects*, 1199(1), 59-64.
- Castelain, C., & Genot, C. (1996). Partition of adsorbed and nonadsorbed bovine serum albumin in dodecane-in-water emulsions calculated from front-face intrinsic fluorescence measurements. *Journal of Agricultural and Food Chemistry*, 44(7), 1635-1640.
- Contado, C., Mehn, D., Gilliland, D., & Calzolari, L. (2019). Characterization methods for studying protein adsorption on nano-polystyrene beads. *Journal of Chromatography A*, 1606.
- Cowsill, B. J., Coffey, P. D., Yaseen, M., Waigh, T. A., Freeman, N. J., & Lu, J. R. (2011). Measurement of the thickness of ultra-thin adsorbed globular protein layers with dual-polarisation interferometry: a comparison with neutron reflectivity. *Soft Matter*, 7(16), 7223-7230.
- Davantes, A., Nigen, M., Sanchez, C., D'Orlando, A., & Renard, D. (2019). Adsorption of Hyperbranched Arabinogalactan-Proteins from Plant Exudate at the Solid-Liquid Interface. *Colloids and Interfaces*, 3(2).
- Davantès, A., Nigen, M., Sanchez, C., & Renard, D. (2021). Adsorption Behavior of Arabinogalactan-Proteins (AGPs) from Acacia senegal Gum at a Solid-Liquid Interface. *Langmuir*, 37, 10547-10559.
- Dazzi, A., Prater, C. B., Hu, Q., Chase, D. B., Rabolt, J. F., & Marcott, C. (2012). AFM-IR: combining atomic force microscopy and infrared spectroscopy for nanoscale chemical characterization. *Applied spectroscopy*, 66(12), 1365-1384.
- de Vos, W. M., & Lindhoud, S. (2019). Overcharging and charge inversion: Finding the correct explanation(s). *Advances in Colloid and Interface Science*, 274.
- Dickinson, E. (1988). The role of hydrocolloids in stabilising particulate dispersions and emulsions. In G. O. Phillips, P. A. Williams & D. J. Wedlock (Eds.), *Gums and Stabilisers for the Food Industry* 4 (pp. 249-263). Oxford: IRL Press.

- Dickinson, E. (2003). Hydrocolloids at interfaces and the influence on the properties of dispersed systems. *Food Hydrocolloids*, 17(1), 25-39.
- Dickinson, E. (2008). Interfacial structure and stability of food emulsions as affected by protein-polysaccharide interactions. *Soft Matter*, 4(5), 932-942.
- Dickinson, E., Galazka, V. B., & Anderson, D. M. W. (1991). Emulsifying behavior of gum-arabic .2. Effect of the gum molecular-weight on the emulsion droplet-size distribution. *Carbohydrate Polymers*, 14(4), 385-392.
- Dickinson, E., Murray, B. S., Stainsby, G., & Anderson, D. M. W. (1988). Surface activity and emulsifying behaviour of some Acacia gums. *Food Hydrocolloids*, 2(6), 477-490.
- Dror, Y., Cohen, Y., & Yerushalmi-Rozen, R. (2006). Structure of gum arabic in aqueous solution. *Journal of Polymer Science Part B-Polymer Physics*, 44(22), 3265-3271.
- Firkowska-Boden, I., Helbing, C., Dauben, T. J., Pieper, M., & Jandt, K. D. (2020). How Nanotopography-Induced Conformational Changes of Fibrinogen Affect Platelet Adhesion and Activation. *Langmuir*, 36(39), 11573-11580.
- Flindt, C., Al-Assaf, S., Phillips, G. O., & Williams, P. A. (2005). Studies on acacia exudate gums. Part V. Structural features of Acacia seyal. *Food Hydrocolloids*, 19(4), 687-701.
- Garti, N., & Reichman, D. (1993). Hydrocolloids as food emulsifiers and stabilizers *Food Structure*, 12(4), 411-426.
- Gashua, I. B., Williams, P. A., & Baldwin, T. C. (2016). Molecular characteristics, association and interfacial properties of gum Arabic harvested from both Acacia senegal and Acacia seyal. *Food Hydrocolloids*, 61, 514-522.
- Guo, X. M., Zhang, X. X., Chu, W. B., Jiang, N., & Li, H. (2020). Infrared Spectroscopic Study of Pepsin Secondary Structure Changes on Surfaces. *Chinese Journal of Analytical Chemistry*, 48(9), 1273-1278.
- Hartvig, R. A., van de Weert, M., Ostergaard, J., Jorgensen, L., & Jensen, H. (2011). Protein Adsorption at Charged Surfaces: The Role of Electrostatic Interactions and Interfacial Charge Regulation. *Langmuir*, 27(6), 2634-2643.
- Hippolyte, I. (1998). Protéines glycosylées de galls *in vitro* d'Acacia senegal. Evolution en fonction de différentes conditions de culture et au cours de stress hydriques. In O. Editions (Ed.), *L'acacia au Sénégal* (pp. 273-283). Paris: Campa, C.; Grignon, C.; Gueye, M.; Hamon, S.
- Jayme, M. L., Dunstan, D. E., & Gee, M. L. (1999). Zeta potentials of gum arabic stabilised oil in water emulsions. *Food Hydrocolloids*, 13(6), 459-465.
- Jia, E. N., Zhao, X., Lin, Y., & Su, Z. H. (2020). Protein adsorption on titanium substrates and its effects on platelet adhesion. *Applied Surface Science*, 529.
- Kurouski, D., Dazzi, A., Zenobi, R., & Centrone, A. (2020). Infrared and Raman chemical imaging and spectroscopy at the nanoscale. *Chemical Society Reviews*, 49(11), 3315-3347.
- Lopez-Torrez, L., Nigen, M., Williams, P., Doco, T., & Sanchez, C. (2015). Acacia senegal vs. Acacia seyal gums - Part 1: Composition and structure of hyperbranched plant exudates. *Food Hydrocolloids*, 51, 41-53.
- Lund, M., Akesson, T., & Jonsson, B. (2005). Enhanced protein adsorption due to charge regulation. *Langmuir*, 21(18), 8385-8388.
- Ma, G. J., Ferhan, A. R., Jackman, J. A., & Cho, N. J. (2020). Elucidating How Different Amphipathic Stabilizers Affect BSA Protein Conformational Properties and Adsorption Behavior. *Langmuir*, 36(35), 10606-10614.
- Mahendran, T., Williams, P. A., Phillips, G. O., Al-Assaf, S., & Baldwin, T. C. (2008). New insights into the structural characteristics of the arabinogalactan - Protein (AGP) fraction of gum Arabic. *Journal of Agricultural and Food Chemistry*, 56(19), 9269-9276.
- Mehrabian, H., Snoeijs, J. H., & Harting, J. (2020). Desorption energy of soft particles from a fluid interface. *Soft Matter*, 16(37), 8655-8666.
- Motlagh, S., Ravines, P., Karamallah, K. A., & Ma, Q. F. (2006). The analysis of Acacia gums using electrophoresis. *Food Hydrocolloids*, 20(6), 848-854.

- Nishino, M., Katayama, T., Sakata, M., Al-Assaf, S., & Phillips, G. O. (2012). Effect of AGP on emulsifying properties of gum Arabic. In G. O. P. P. A. W. J.F. Kennedy (Ed.), *Gum Arabic* (pp. 269-274). Cambridge: RSC Publishing.
- Osman, M. E., Menzies, A. R., Williams, P. A., Phillips, G. O., & Baldwin, T. C. (1993). The molecular characterization of the polysaccharide gum from Acacia-Senegal *Carbohydrate Research*, *246*, 303-318.
- Padala, S. R., Williams, P. A., & Phillips, G. O. (2009). Adsorption of Gum Arabic, Egg White Protein, and Their Mixtures at the Oil-Water Interface in Limonene Oil-in-Water Emulsions. *Journal of Agricultural and Food Chemistry*, *57*(11), 4964-4973.
- Parhi, P., Golas, A., Barnthip, N., Noh, H., & Vogler, E. A. (2009). Volumetric interpretation of protein adsorption: Capacity scaling with adsorbate molecular weight and adsorbent surface energy. *Biomaterials*, *30*(36), 6814-6824.
- Rampon, V., Brossard, C., Mouhous-Riou, N., Bousseau, B., Llamas, G., & Genot, C. (2004). The nature of the apolar phase influences the structure of the protein emulsifier in oil-in-water emulsions stabilized by bovine serum albumin. A front-surface fluorescence study. *Advances in Colloid and Interface Science*, *108*, 87-94.
- Randall, R. C., Phillips, G. O., & Williams, P. A. (1988). The role of the proteinaceous component on the emulsifying properties of gum arabic. *Food Hydrocolloids*, *2*(2), 131-140.
- Razumovsky, L., & Damodaran, S. (1999). Surface activity-compressibility relationship of proteins at the air-water interface. *Langmuir*, *15*(4), 1392-1399.
- Redgwell, R. J., Schmitt, C., Beaulieu, M., & Curti, D. (2005). Hydrocolloids from coffee: physicochemical and functional properties of an arabinogalactan-protein fraction from green beans. *Food Hydrocolloids*, *19*(6), 1005-1015.
- Renard, D., Garnier, C., Lapp, A., Schmitt, C., & Sanchez, C. (2012). Structure of arabinogalactan-protein from Acacia gum: From porous ellipsoids to supramolecular architectures. *Carbohydrate Polymers*, *90*(1), 322-332.
- Renard, D., Garnier, C., Lapp, A., Schmitt, C., & Sanchez, C. (2013). Structure of arabinogalactan-protein from Acacia gum: From porous ellipsoids to supramolecular architectures (vol 90, pg 322, 2012). *Carbohydrate Polymers*, *97*(2), 864-867.
- Renard, D., Lavenant-Gourgeon, L., Lapp, A., Nigen, M., & Sanchez, C. (2014). Enzymatic hydrolysis studies of arabinogalactan-protein structure from Acacia gum: The self-similarity hypothesis of assembly from a common building block. *Carbohydrate Polymers*, *112*, 648-661.
- Renard, D., Lavenant-Gourgeon, L., Ralet, M. C., & Sanchez, C. (2006). Acacia senegal gum: Continuum of molecular species differing by their protein to sugar ratio, molecular weight, and charges. *Biomacromolecules*, *7*(9), 2637-2649.
- Roach, P., Farrar, D., & Perry, C. C. (2005). Interpretation of protein adsorption: Surface-induced conformational changes. *Journal of the American Chemical Society*, *127*(22), 8168-8173.
- Roach, P., Farrar, D., & Perry, C. C. (2006). Surface tailoring for controlled protein adsorption: Effect of topography at the nanometer scale and chemistry. *Journal of the American Chemical Society*, *128*(12), 3939-3945.
- Sabet, S., Rashidinejad, A., Melton, L. D., Zujovic, Z., Akbarinejad, A., Nieuwoudt, M., Seal, C. K., & McGillivray, D. J. (2021). The interactions between the two negatively charged polysaccharides: Gum Arabic and alginate. *Food Hydrocolloids*, *112*.
- Sanchez, C., Nigen, M., Tamayo, V. M., Doco, T., Williams, P., Amine, C., & Renard, D. (2018). Acacia gum: History of the future. *Food Hydrocolloids*, *78*, 140-160.
- Sanchez, C., Schmitt, C., Kolodziejczyk, E., Lapp, A., Gaillard, C., & Renard, D. (2008). The acacia gum arabinogalactan fraction is a thin oblate ellipsoid: A new model based on small-angle neutron scattering and ab initio calculation. *Biophysical Journal*, *94*(2), 629-639.
- Snowden, M. J., Phillips, G. O., & Williams, P. A. (1987). Functional characteristics of gum arabic. *Food Hydrocolloids*, *1*(4), 291-300.

- Snowden, M. J., Phillips, G. O., & Williams, P. A. (1988). Adsorption and stabilising properties of gum arabic samples of different origin. In G. O. Phillips, P. A. Williams & D. J. Wedlock (Eds.), *Gums and Stabilisers for the Food Industry 4* (pp. 489-496). Oxford: IRL Press.
- Song, J. K., Choi, H. J., & Chin, I. (2007). Preparation and properties of electrophoretic microcapsules for electronic paper. *Journal of Microencapsulation*, *24*(1), 11-19.
- Tamayo, V. M. (2018). *Propriétés volumétriques des Arabinogalactane-protéines d'exsudats de gommages d'Acacia*. Université de Montpellier.
- Tamayo, V. M., Nigen, M., Apolinar-Valiente, R., Doco, T., Williams, P., Renard, D., & Sanchez, C. (2018). Flexibility and Hydration of Amphiphilic Hyperbranched Arabinogalactan-Protein from Plant Exudate: A Volumetric Perspective. *Colloids and Interfaces*, *2*(1).
- Tian, Y., Zhang, Z., Zhang, P. P., Taha, A., Hu, H., & Pan, S. Y. (2020). The role of conformational state of pH-shifted beta-conglycinin on the oil/water interfacial properties and emulsifying capacities. *Food Hydrocolloids*, *108*.
- Trindade, J. R., Freire, M. G., Amaral, P. F. F., Coelho, M. A. Z., Coutinho, J. A. P., & Marrucho, I. M. (2008). Aging mechanisms of oil-in-water emulsions based on a bioemulsifier produced by *Yarrowia lipolytica*. *Colloids and Surfaces a-Physicochemical and Engineering Aspects*, *324*(1-3), 149-154.
- Verbeken, D., Dierckx, S., & Dewettinck, K. (2003). Exudate gums: occurrence, production, and applications. *Applied Microbiology and Biotechnology*, *63*(1), 10-21.
- Vogler, E. A. (2012). Protein adsorption in three dimensions. *Biomaterials*, *33*(5), 1201-1237.
- Wang, D. W., & Zhao, X. P. (2009). Microencapsulated electric ink using gelatin/gum arabic. *Journal of Microencapsulation*, *26*(1), 37-45.
- Wang, Q., Burchard, W., Cui, S. W., Huang, X. Q., & Phillips, G. O. (2008). Solution properties of conventional gum arabic and a matured gum arabic (*Acacia* (sen) SUPER GUM). *Biomacromolecules*, *9*(4), 1163-1169.
- Wang, S. N., Yang, J. J., Shao, G. Q., Liu, J., Wang, J., Yang, L. N., Li, J., Liu, H., Zhu, D. S., Li, Y., & Jiang, L. Z. (2020). pH-induced conformational changes and interfacial dilatational rheology of soy protein isolated/soy hull polysaccharide complex and its effects on emulsion stabilization. *Food Hydrocolloids*, *109*.
- Wasilewska, M., & Adamczyk, Z. (2011). Fibrinogen Adsorption on Mica Studied by AFM and in Situ Streaming Potential Measurements. *Langmuir*, *27*(2), 686-696.
- Yadav, M. P., Igartuburu, J. M., Yan, Y. C., & Nothnagel, E. A. (2007). Chemical investigation of the structural basis of the emulsifying activity of gum arabic. *Food Hydrocolloids*, *21*(2), 297-308.
- Zeliszewska, P., Bratek-Skicki, A., Adamczyk, Z., & Ciesla, M. (2014). Human Fibrinogen Adsorption on Positively Charged Latex Particles. *Langmuir*, *30*(37), 11165-11174.
- Zhai, J. L., Day, L., Aguilar, M. I., & Wooster, T. J. (2013). Protein folding at emulsion oil/water interfaces. *Current Opinion in Colloid & Interface Science*, *18*(4), 257-271.
- Zhang, L. A., Pelton, R., Ketelson, H., & Meadows, D. (2011). Charge regulation enables anionic hydroxypropyl guar-borate adsorption onto anionic and cationic polystyrene latex. *Journal of Colloid and Interface Science*, *353*(2), 557-561.

Table 1. Summary of molecular properties of raw materials used in this study

	<i>A. senegal</i> ^a	<i>A. seyal</i> ^a	HIC-FI ^a	HIC-FII ^a	HIC-FIII ^a
Protein content (%)	2.4	0.8	1	9	25
M _w (g/mol)	6.86 10 ⁵	8.31 10 ⁵	2.80 10 ⁵	1.86 10 ⁶	1.59 10 ⁶
D _h (nm) ^b	25	25	18	69	32
ζ (mV) ^c	-25.2	-11.6	nd	nd	nd
Number of charges ^d					
Polysaccharide substitutions	402	147	223	1149	609
Polypeptide backbone	30	11	0	110	996
Positive charges	17	6	0	70	329
Negative charges	13	5	0	40	667
Average number of charges / AGP	432	158	223	1249	1605
	Latex	Latex Amino	Latex Carboxy	Latex Amidine	
Manufacturer	Sigma-Aldrich	Polysciences	Invitrogen	Invitrogen	
D _h (nm) ^b	117 +/- 2.4	469 +/- 7.4	114 +/- 1.5	102 +/- 0.9	
ζ (mV) ^c	-43.2	-19.6	-39.9	+52.2	
Average number of charges / particle ^e	-214	-428	-185	+198	
ζ _{latex} / ζ _{GA}					
<i>A. senegal</i>	1.7	0.8	1.6	2.1	
<i>A. seyal</i>	3.7	1.7	3.4	4.5	

^a Protein contents from *A. senegal* molecular fractions isolated from hydrophobic interaction chromatography (HIC) were given in Renard et al. (2006); protein contents from *A. senegal* and *A. seyal* gums were given in Lopez-Torrez et al. (2015)

^b Hydrodynamic diameters were calculated from sphere-equivalent hydrodynamic radius determined at pH 5.82 in water by dynamic light scattering using the cumulant method

^c ζ potential values taken at pH 5.82. Negative ζ potential value of bare latex and amino latex particles in agreement with carboxylic (COO⁻) and sulfate (SO₄²⁻) residual groups present at the surface (as stated by the manufacturer)

^d from Table 2 and Table 6 in Renard et al. (2006); number of charges of *A. seyal* estimated from biochemical composition and ζ value comparison between *A. senegal* and *A. seyal*

^e from the Lorentz-Stokes relationship $N_c = (6 \cdot \pi \cdot \eta \cdot 10^8 / 1.602) \cdot R_h \cdot \mu_e$ (less accurate however if $\kappa a > 1$, i.e. for $I > 3 \cdot 10^{-5}$ M and $R_h = 55$ nm)

Table 2. Molecular properties of Acacia gum (GA) coated latex (carboxy or amidine) at C = 0.0025% and pH 5.82 as a function of GA concentration using asymmetric flow field flow fractionation (A4F) method

GA (%) GA (ppm)	0	0.00095 9.5	0.00475 47.5	0.0095 95	0.0475 475	0.095 950
• Latex carboxy / GA Senegal •						
M_w (g.mol ⁻¹)	4.2 10 ⁸	4.51 10 ⁸	4.81 10 ⁸	5.11 10 ⁸	7.22 10 ⁸	9.55 10 ⁸
M_w/M_n	1.005	1.003	1.002	1.003	1.007	1.004
R_g (nm)	47.4	47.5	47.8	48	48.6	48.7
δ (nm)*	0	1.9	10.3	20.8	69.1	77.6
Number of GA adsorbed**	0	34	77	122	429	769
Area _{latex} /Area _{GA adsorbed} ***	0	2.45	1.08	0.68	0.19	0.11
Surface coverage		0.41	0.93	1.47	5.16	9.25
Structure layer		Partial coverage	monolayer	multilayer		
• Latex carboxy / GA Seyal •						
M_w (g.mol ⁻¹)	4.2 10 ⁸	4.61 10 ⁸	5.09 10 ⁸	5.51 10 ⁸	7.08 10 ⁸	8.56 10 ⁸
M_w/M_n	1.005	1.003	1.001	1.002	1.001	1.006
R_g (nm)	47.4	47.4	47.5	47.7	47.8	48.4
δ (nm)*	0	1.4	2.3	3.5	6.1	6.4
Number of GA adsorbed**	0	40	98	148	337	516
Area _{latex} /Area _{GA adsorbed} ***	0	2.08	0.85	0.56	0.25	0.16
Surface coverage		0.48	1.18	1.78	4.05	6.20
Structure layer		Partial coverage	monolayer	multilayer		
• Latex amidine / GA Senegal •						
M_w (g.mol ⁻¹)	3.37 10 ⁷	7.6 10 ⁸	7.87 10 ⁸	8.90 10 ⁸	1.33 10 ⁹	1.51 10 ⁹
M_w/M_n	1.041	1.224	1.194	1.189	1.242	1.238
R_g (nm)	59.9	80.5	87.2	84	76.2	74.6
δ (nm)*	0	11.7	13.9	17.9	24.3	34.5
Number of GA adsorbed**	0	1059	1098	1249	1882	2158
Area _{latex} /Area _{GA adsorbed} ***	0	0.063	0.061	0.053	0.035	0.031
Surface coverage		15.9	16.5	18.8	28.3	32.4
Structure layer		multilayer				
• Latex amidine / GA Seyal •						
M_w (g.mol ⁻¹)	3.37 10 ⁷	7.61 10 ⁸	5.54 10 ⁸	5.35 10 ⁸	4.57 10 ⁸	4.19 10 ⁸
M_w/M_n	1.041	1.293	1.168	1.196	1.131	1.117
R_g (nm)	59.9	113	87	71	68	65.1
δ (nm)*	0	14.7	15.5	16.5	19.8	21.2
Number of GA adsorbed**	0	875	626	603	509	463
Area _{latex} /Area _{GA adsorbed} ***	0	0.076	0.106	0.110	0.131	0.144
Surface coverage		10.5	7.5	7.2	6.1	5.6
Structure layer		multilayer				

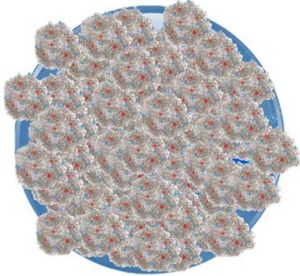
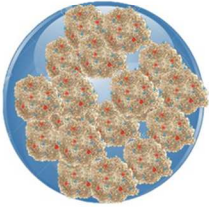
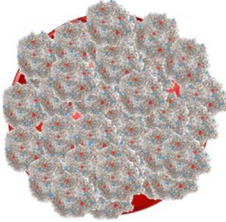
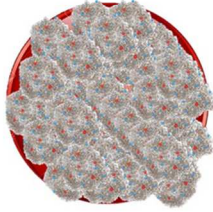
*From DLS **From $(M_w(\text{Latex} + \text{GA}) - M_w(\text{Latex}) / M_w(\text{GA}))$ with $M_w(\text{GA Senegal}) = 6.86 \cdot 10^5$ g.mol⁻¹ and $M_w(\text{GA Seyal}) = 8.31 \cdot 10^5$ g.mol⁻¹ *** Area calculated from $A = \pi \cdot R_h^2$

Table 3. Adsorbed layer thickness δ (nm) and zeta potential ξ (mV) of 0.1 μm latex particles and 0.5 μm latex amino particles after 14 and 11 days of adsorption, respectively, in water ($C = 0.025\%$) coated by *A. senegal* or *A. seyal* gums or *A. senegal* molecular fractions. Protein content for each sample was also reported.

0.1 μm latex particles												
Sample	Latex	<i>A. seyal</i>	<i>A. senegal</i>	<i>Latex + A. seyal</i>	<i>Latex + A. senegal</i>	<i>Latex + A. seyal</i>	<i>Latex + HIC-FI</i>	<i>Latex + HIC-FIII</i>	<i>Latex + HIC-FII</i>	<i>Latex + A. senegal</i>	<i>Latex + HIC-FIII</i>	<i>Latex + HIC-FII</i>
concentration (%)	0.5	1	1	0.01	0.01	0.05	0.05	0.003	0.01	0.05	0.01	0.05
Protein content (%) ^a	-			0.008	0.024	0.04	0.05	0.075	0.09	0.12	0.25	0.45
δ (nm)	-	-	-	3.6	19.2	5.1	8	7.6	25.1	62.3	178.0	230.8
ξ (mV)	-43.2	-11.6	-23.7	-42.1	-38.1	-28.9	-25.6	-39.5	-51.2	-25.7	-33.0	-48.3
0.5 μm latex amino particles												
Sample	Latex	<i>Latex + A. seyal</i>	<i>Latex + A. senegal</i>	<i>Latex + A. seyal</i>	<i>Latex + A. senegal</i>							
Concentration (%)	0.5	0.01	0.01	0.05	0.05							
Protein content (%)	-	0.008	0.024	0.04	0.12							
δ (nm)	-	10.4	57.6	15.3	143.3							
Ratio		2.9	3.0	3.0	2.3							
$\delta_{\text{amino latex}} / \delta_{\text{latex}}$												
ξ (mV) ^c		-19.6	-12.1	-21.7	-11.9	-22.9						

^a Protein contents from *A. senegal* molecular fractions were given in Renard *et al.* (2006); protein contents from *A. senegal* and *A. seyal* gums were given in Lopez-Torrez *et al.* (2015)

Table 4. Summary of adsorption properties of *A. senegal* and *A. seyal* gums onto latex particles.

Latex	Carboxy	Carboxy	Amidine	Amidine
Number of charges	-185	-185	+198	+198
GA	<i>A. senegal</i>	<i>A. seyal</i>	<i>A. senegal</i>	<i>A. seyal</i>
Number of charges	432	158*	432	158*
Polysaccharide substitution	402	147	402	147
Polypeptide backbone	30	11	30	11
Positive charges	17	6	17	6
Negative charges	13	5	13	5
Adsorption	High	Weak	Medium	Medium
Layer thickness	High	Weak	Medium	Medium
Number of GA adsorbed	Medium	Weak	High	Medium
Hydration	High	Weak	Medium	Medium
Model				
	Carboxy/Senegal	Carboxy/Seyal	Amidine/Senegal	Amidine/Seyal

* number of charges estimated from ζ value comparison between *A. senegal* and *A. seyal*


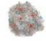


Legend				
	Latex carboxy	<i>A. senegal</i>	<i>A. seyal</i>	Latex amidine

Figure captions

Figure 1. (a) (b) Adsorbed layer thickness δ (nm) and (c) (d) zeta potential ζ (mV) of carboxy and amidine latex particles ($C = 0.025\%$) coated with *A. senegal* or *A. seyal* gums (GA) as a function of GA concentration or protein content (%) at pH 5.82 after 15 days of equilibration. Horizontal dotted lines indicate ζ potential values of *A. senegal* and *A. seyal* alone.

(■) Latex carboxy / *A. senegal*; (●) Latex carboxy / *A. seyal*; (□) Latex amidine / *A. senegal*; (○) Latex amidine / *A. seyal*

Figure 2. STEM images of bare carboxy latex (a) and carboxy latex – *A. senegal* dispersions (b, c, d, e) clearly revealing the deflocculation process of latex particles after GA addition.

Scale bars: 5 μm (a), 1 μm (b), 300 nm (c), 300 nm (d), 200 nm (e)

Figure 3. (a) Relationship between the adsorbed layer thickness δ (nm) (determined by Dynamic Light Scattering) as a function of the number of adsorbed GA macromolecules per carboxy or amidine latex particle (determined using Asymmetrical Flow Field Fractionation). (b) Relationship between the ratio R_g/R_h of carboxy and amidine latex particles after GA adsorption as a function of the number of adsorbed GA macromolecules per carboxy or amidine latex particle

(■) Latex carboxy / GA *senegal*; (●) Latex carboxy / GA *seyal*; (■) Latex amidine / GA *senegal*; (●) Latex amidine / GA *seyal*

Figure 4. Adsorbed layer thickness δ (nm) and zeta potential ζ (mV) after 12 or 14 days of equilibration of (a, b) carboxy and (c, d) amidine latex particles ($C = 0.025\%$) in water coated with gum (*A. senegal* or *A. seyal*, $C = 0.0475\%$) as a function of pH (). ζ potential values of *A. senegal* and *A. seyal* alone as a function of pH are also indicated.

(□) + *A. seyal* pH 4.32; (◇) + *A. seyal* pH 6.33; (<) + *A. seyal* pH 6.25; (■) + *A. senegal* pH 4.08; (●) + *A. senegal* pH 4.98; (◀) + *A. senegal* pH 6.00

Figure 5. (a) Adsorbed layer thickness δ (nm) of 0.1 μm latex particles in water ($C = 0.025\%$) coated with gum (*A. senegal* or *A. seyal*) or *A. senegal* molecular fractions at pH 5.9 as a function of time (days). (○) + *A. seyal* 0.01%; (□) + *A. seyal* 0.05%; (●) + *A. senegal* 0.01%; (■) + *A. senegal* 0.05%; (▲) + HIC-FI 0.05%; (▼) + HIC-FII 0.01%; (◆) HIC-FII 0.05%; (◄) + HIC-FIII 0.003%; (►) HIC-FIII 0.01% (b) Adsorbed layer thickness δ (nm) of 0.5 μm amino latex particles in water ($C = 0.025\%$) coated with (■) *A. senegal* 0.01%, (●) *A. senegal* 0.05%, (□) *A. seyal* 0.01% and (○) *A. seyal* 0.05% as a function of time (c) adsorbed layer thickness of 0.1 μm latex particles as a function of protein content (%)

Figure 6. Infrared spectra of latex and Acacia gums in bulk and adsorbed onto latex particles (B) using IR (A) and nanoIR (B) spectroscopy. (A) (—) latex, (—) *A. senegal*, (—) *A. seyal*; (B) (—) latex, (—) *A. senegal*, (—) *A. senegal* adsorbed onto latex particles (—) *A. seyal* adsorbed onto latex particles

Figure 7. Atomic force microscopy images coupled to infrared spectroscopy (NanoIR) of gum alone, bare latex particles and gum (*A. senegal* or *A. seyal*) coated latex particles (Sigma). Topographical images 5x5 μm^2 (a, b) or 3x3 μm^2 (d, h) or 0.2x0.2 μm^2 (f, j) and IR mapping

images at 1654 cm^{-1} (c, e, g, i, k) based on IR spectra of each sample. For the nanoIR mapping the color scales are in arbitrary units, yellow being the maximum of intensity

Figure 8. NanoIR spectroscopy and AFM images of *A. senegal* molecular fractions (F1, F2, F3) adsorbed onto latex particles. (—) latex, (—) HIC-FI + latex, (—) HIC-FII + latex, (—) HIC-FIII + latex. Topographical images $3 \times 3\ \mu\text{m}^2$ (a, c, e) and IR mapping images at 1654 cm^{-1} (b, d, f) based on IR spectra of each sample

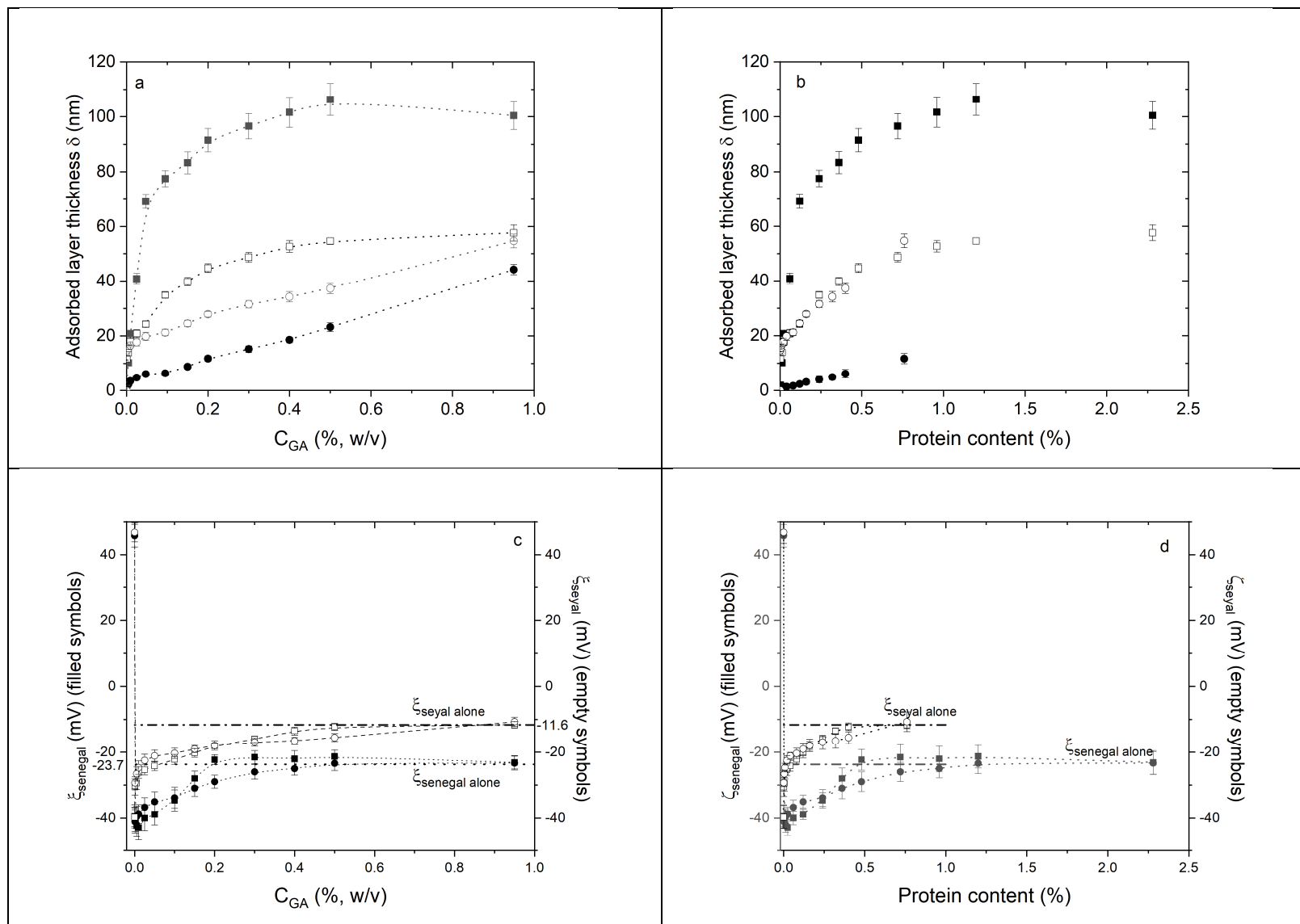


Figure 1 expanded

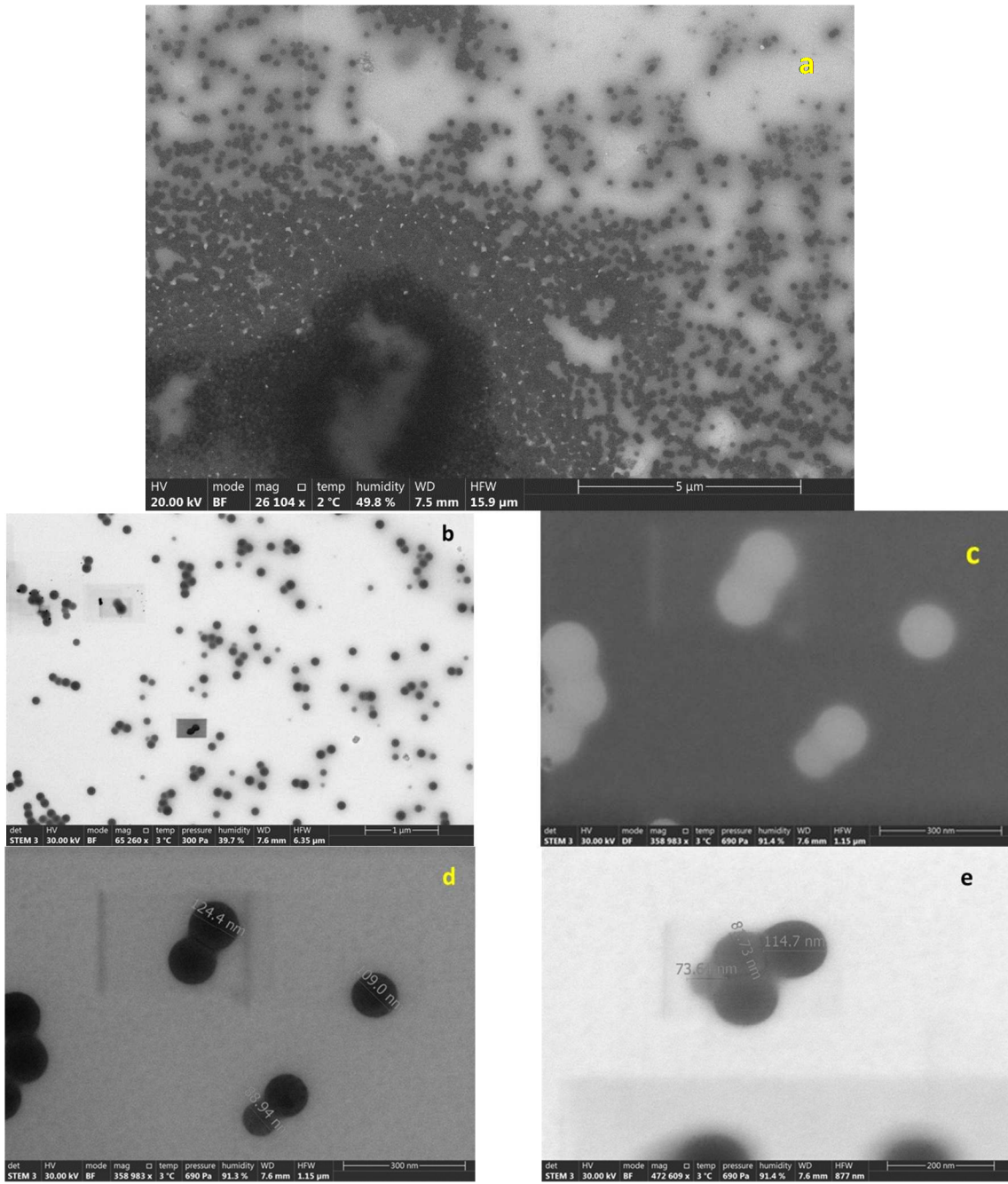
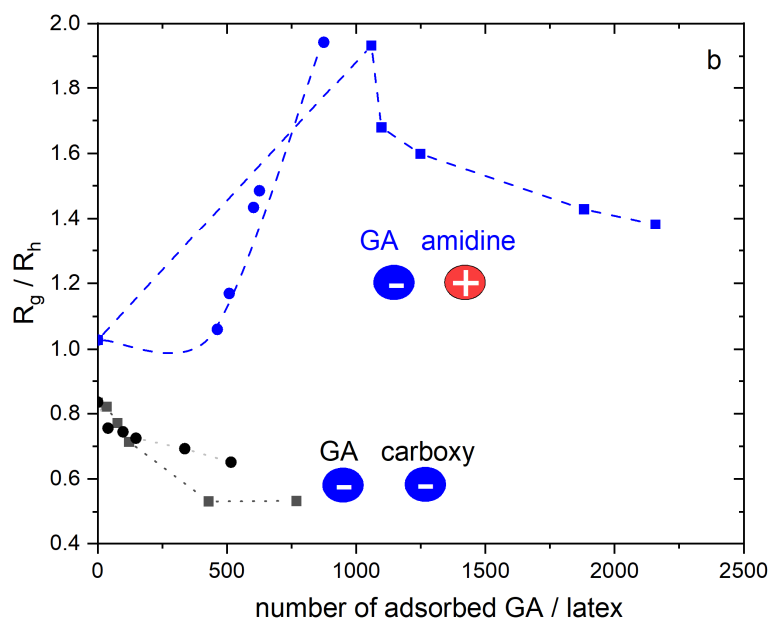
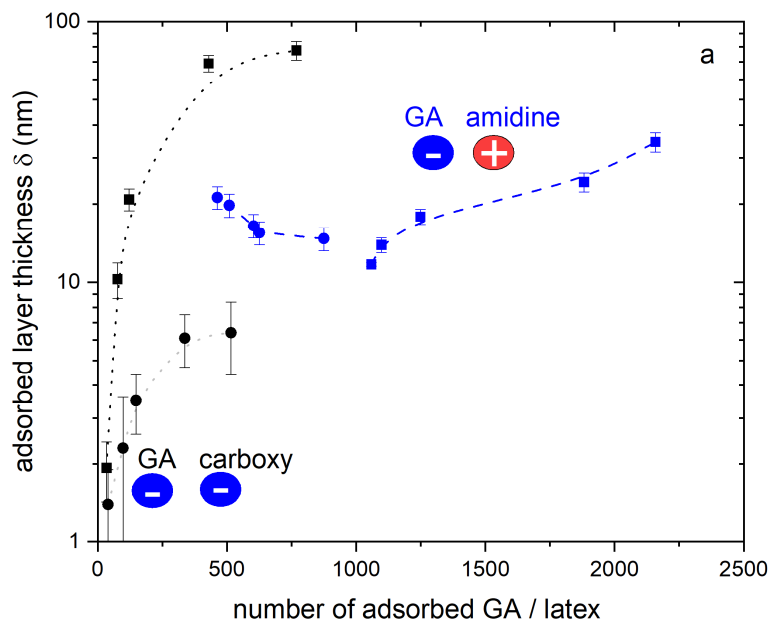
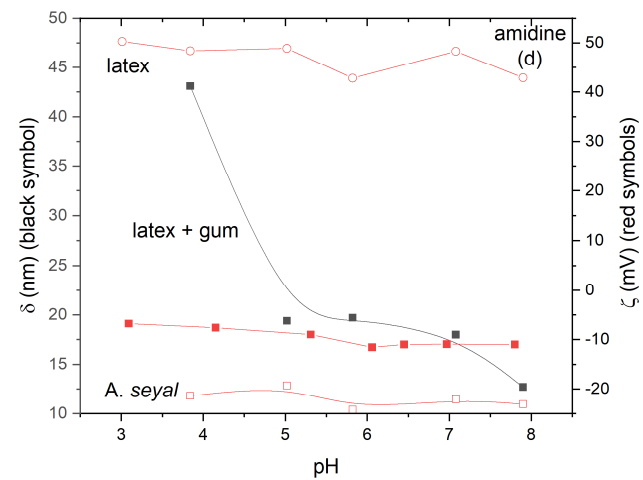
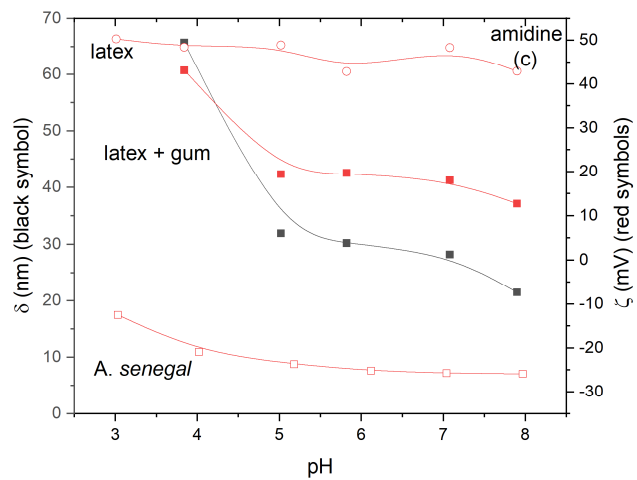
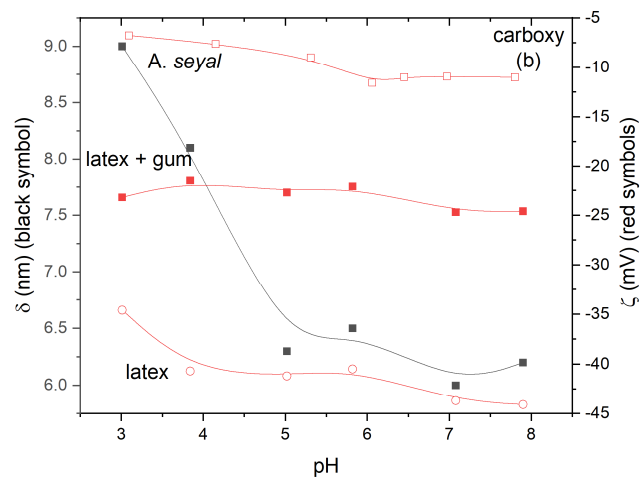
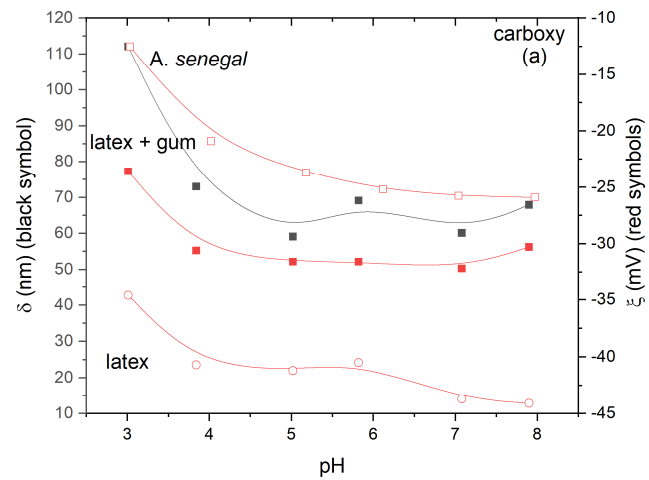


Figure 2



Figure



New Figure 4

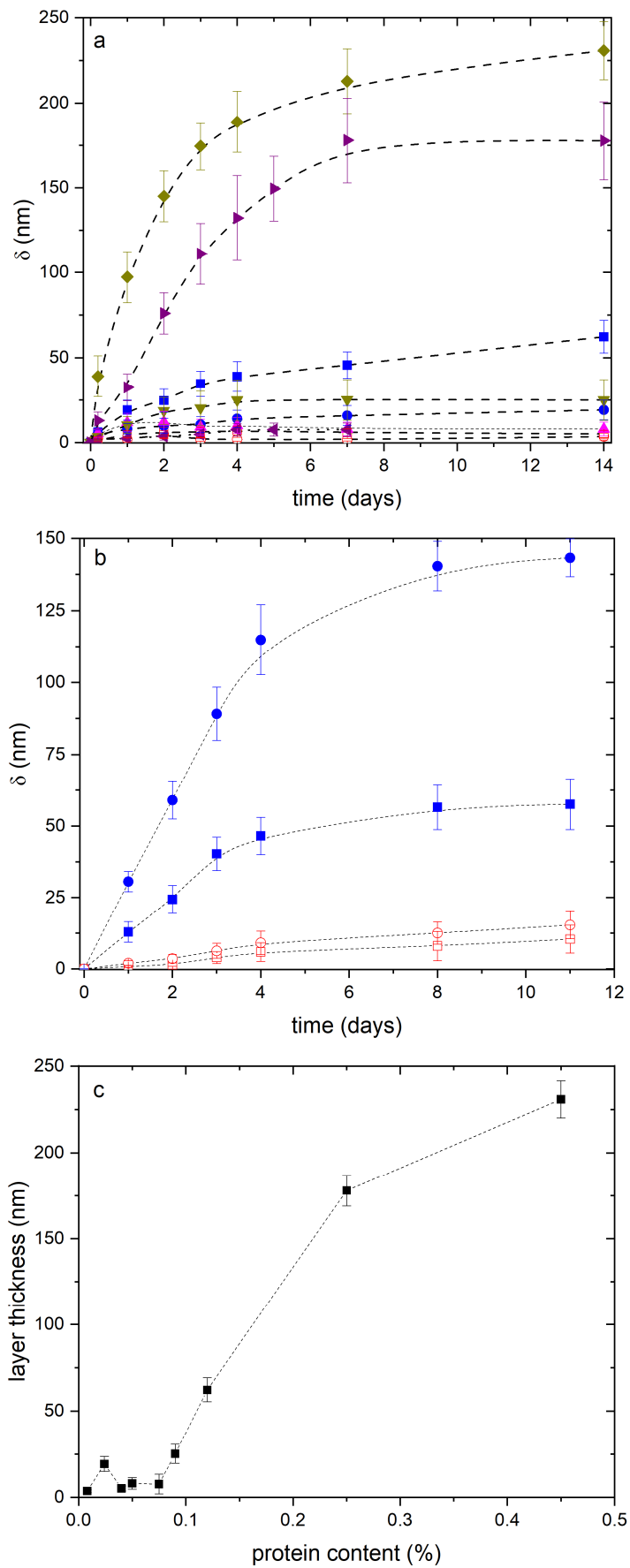


Figure 5

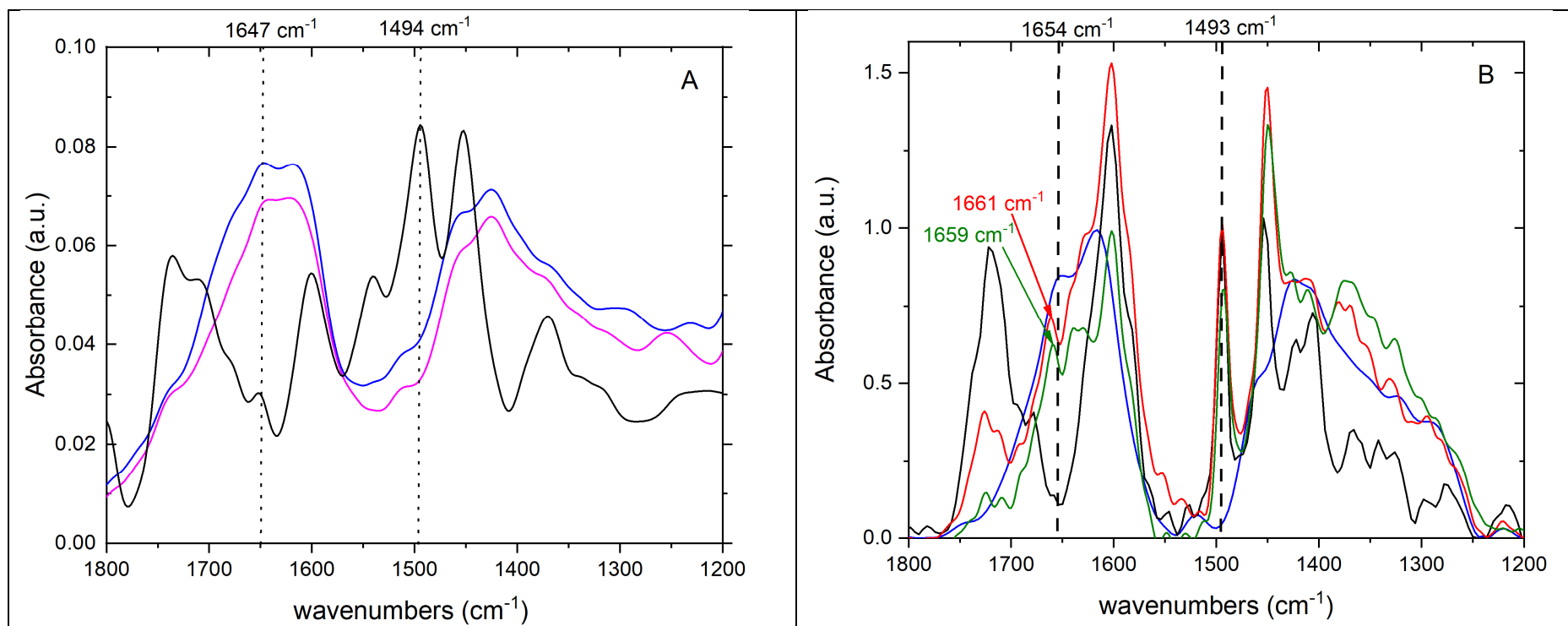


Figure 6

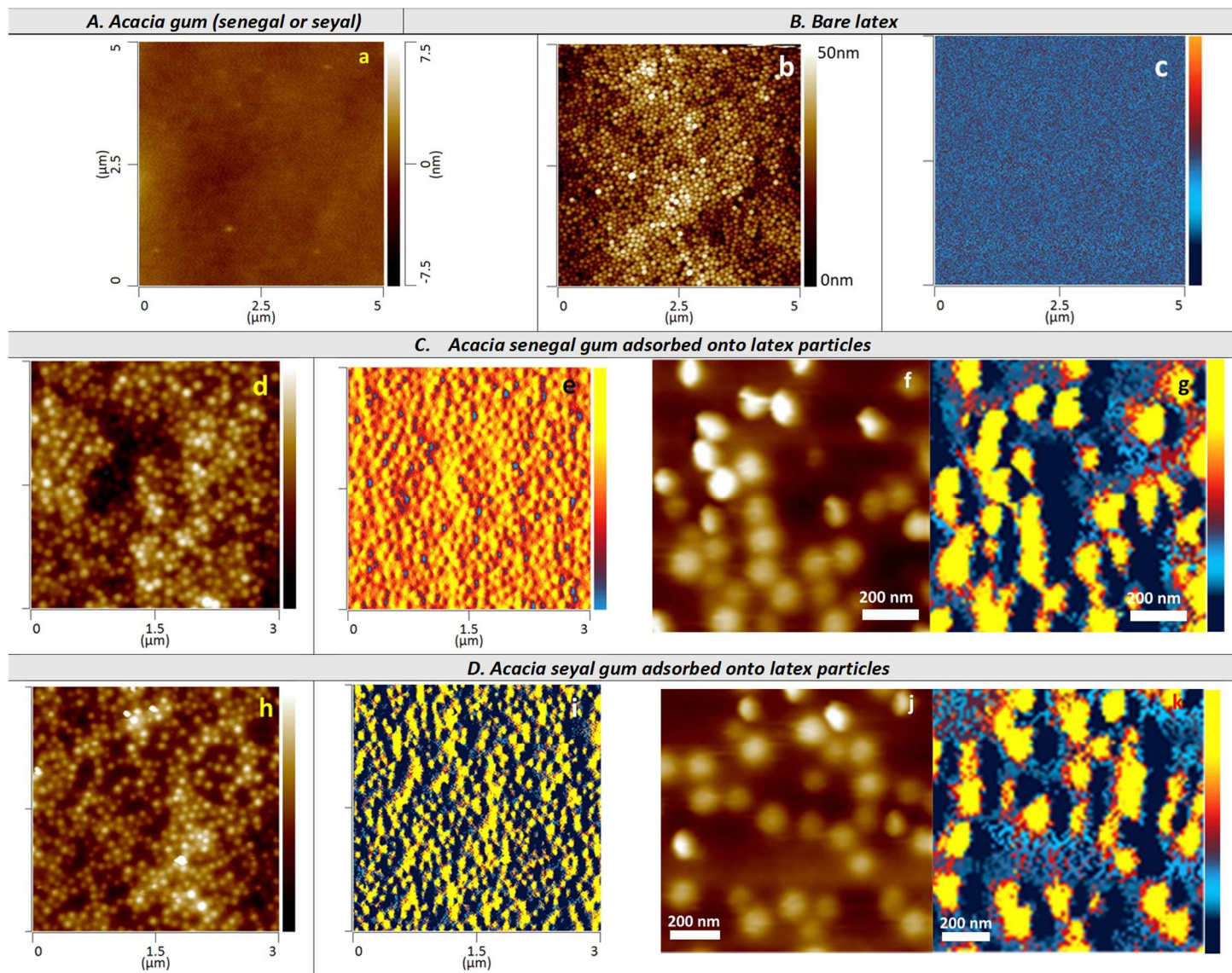


Figure 7

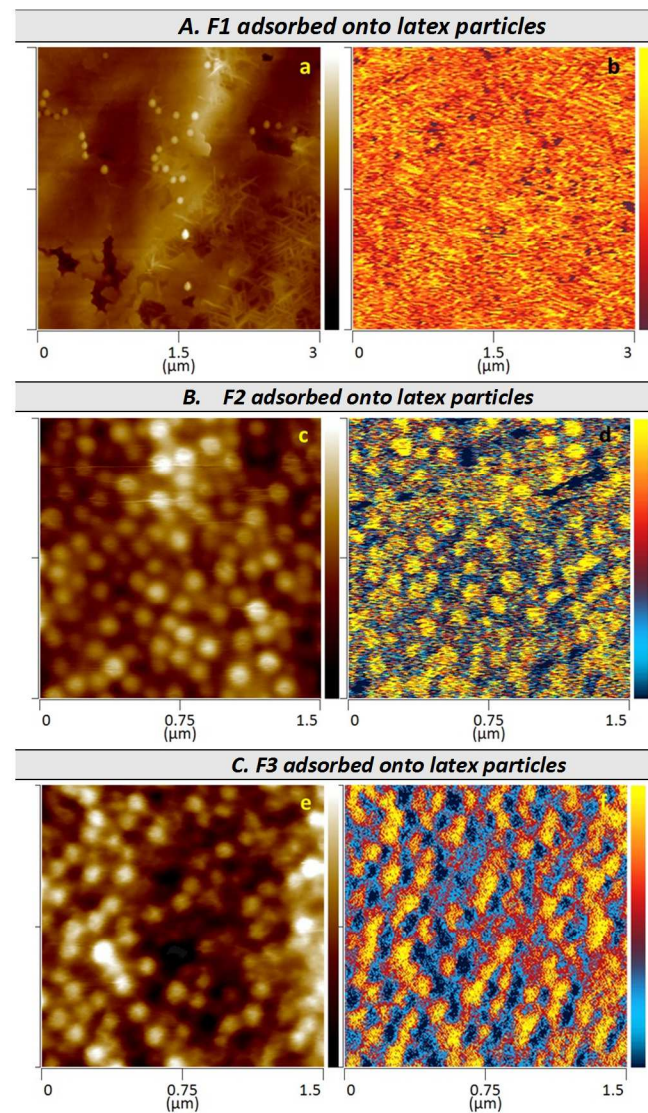
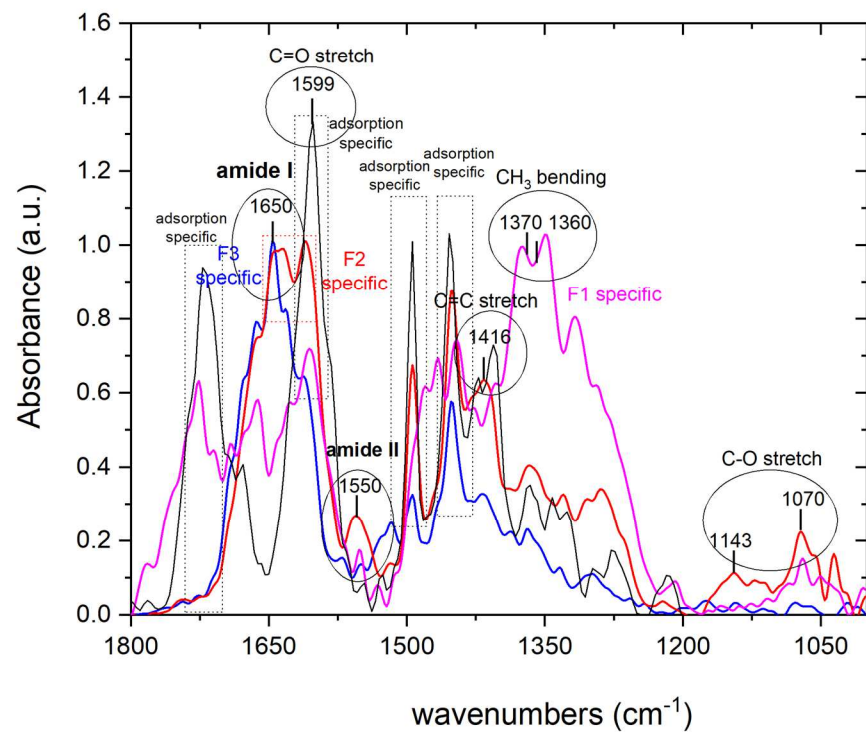


Figure 8

Graphical abstract

